

AD-763 207

EROSION STUDY OF 7.6 CR-MO-V STEEL GUN  
TUBES. PART I. EROSION ANALYSIS AND  
CHARACTERIZATION. PART II. FATIGUE  
BEHAVIOR IN REACTIVE ENVIRONMENTS

Robert C. Tooke, et al

Missouri University

Prepared for:

Army Weapons Command

April 1973

DISTRIBUTED BY:

**NTIS**

National Technical Information Service  
U. S. DEPARTMENT OF COMMERCE  
5285 Port Royal Road, Springfield Va. 22151

**Best  
Available  
Copy**

AD 763207

R-RR-T-1-12-73

AD

# **EROSION STUDY OF 7.62MM CR-MO-V STEEL GUN TUBES**

**PART I. Erosion Analysis and Characterization**

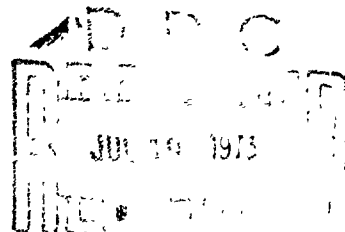
**PART II. Fatigue Behavior in Reactive Environments**



## **TECHNICAL REPORT**

April 1973

NATIONAL TECHNICAL  
INFORMATION SERVICE



## **RESEARCH DIRECTORATE**

WEAPONS LABORATORY, ROCK ISLAND ARSENAL

Rock Island, Illinois 61201

Approved for public release, distribution unlimited.

**DISPOSITION INSTRUCTIONS:**

Destroy this report when it is no longer needed. Do not return it to the originator.

**DISCLAIMER:**

The findings of this report are not to be construed as an official Department of the Army position unless so designated by other authorized documents.

ACCESSION for	
NTIS	White Section <input checked="" type="checkbox"/>
DDC	Buff Section <input type="checkbox"/>
UNANNOUNCED	<input type="checkbox"/>
JUSTIFICATION .....	
BY	
DISTRIBUTION/AVAILABILITY CODES	
Dis.	Accession
A	

Unclassified

Security Classification

## DOCUMENT CONTROL DATA - R &amp; D

(Security classification of title, body of abstract and indexing annotation must be entered when the overall report is classified)

1. ORIGINATING ACTIVITY (Corporate author) Graduate Center for Materials Research Space Sciences Research Center University of Missouri - Rolla, Missouri 65401		2a. REPORT SECURITY CLASSIFICATION Unclassified	
3. REPORT TITLE EROSION STUDY OF 7.62MM CR-MO-V STEEL GUN TUBES PART I. Erosion Analysis and Characterization PART II. Fatigue Behavior in Reactive Environments		2b. GROUP	
4. DESCRIPTIVE NOTES (Type of report and inclusive dates) Technical Report			
5. AUTHOR(S) (First name, middle initial, last name) Robert C. Tooke and Thomas J. O'Keefe			
6. REPORT DATE April 1973		7a. TOTAL NO. OF PAGES 114	7b. NO. OF REFS 33
8a. CONTRACT OR GRANT NO. DAAF01-69-C-0541		9a. ORIGINATOR'S REPORT NUMBER(S)	
b. PROJECT NO. AMS Code 5524.11.80700.03		9b. OTHER REPORT NO(S) (Any other numbers that may be assigned this report) R-RR-T-1-12-73	
10. DISTRIBUTION STATEMENT Approved for public release, distribution unlimited.			
11. SUPPLEMENTARY NOTES this document may be better studied on microfiche.		12. SPONSORING MILITARY ACTIVITY Research Directorate Weapons Laboratory, RIA Rock Island, Illinois 61201	
13. ABSTRACT As a segment of a small arms program at the Research Directorate, Weapons Laboratory, Rock Island Arsenal, the erosion process in 7.62mm steel gun barrels has been chronologically characterized by investigation of the test-fired barrels fired from 1 to 3000 rounds. Both unplated barrels and barrels with hard chromium plated bores were included. Detailed metallurgical analysis, using modern analytical techniques, was conducted on the test-fired gun barrels. Evidence is presented to demonstrate that chemical effects substantially augment the erosion phenomenon caused by thermomechanical factors. Gas-metal reactions and chemical attack involving Pb, S, Cu (Cu-Zn) and Ca comprise the observed chemical effects. Although the chromium plating resists chemical attack of the underlying steel, inherent defects in the plating act as crack initiators. Cracks propagate from the plating defects into the steel moving both laterally and radially to cause removal of plating fragments and eventual rupture of the gun tube. In addition to the contribution to crack propagation, chemical effects are in evidence uniformly over the entire bore surface of unplated barrels. To complement the erosion analysis, cantilever-fatigue tests on unplated and Cr-plated Cr-Mo-V steel specimens in reactive environments at elevated temperatures were conducted. The analysis of the cracking phenomenon in reactive environments included an examination of the role of chromium plating in reducing fatigue life. (U) (Tooke, R.C. and O'Keefe, T.J.)			

DD FORM 1473

REPLACES DD FORM 1473, 1 JAN 64, WHICH IS OBSOLETE FOR ARMY USE.

Unclassified

Security Classification

Unclassified

Security Classification

14	KEY WORDS	LINK A		LINK B		LINK C	
		ROLE	WT	ROLE	WT	ROLE	WT
	1. Gun Tube Erosion						
	2. Erosion Analysis						
	3. Fatigue						
	4. Crack Propagation						
	5. Gas-Steel Reactivity						

Unclassified

Security Classification

RESEARCH DIRECTORATE  
WEAPONS LABORATORY, RIA  
ROCK ISLAND ARSENAL  
ROCK ISLAND, ILLINOIS

TECHNICAL REPORT  
R-RR-T-1-12-73

EROSION STUDY OF 7.62MM CR-MO-V STEEL GUN TUBES

PART I. Erosion Analysis and Characterization

PART II Fatigue Behavior in Reactive Environments

April 1973

Contract DAAF01-69-C-0541

AMS Code 5524.11.80700.03

Approved for public release, distribution unlimited.

i *h*

## FOREWORD

This report was prepared by Dr. R. C. Tooke and Professor T. J. O'Keefe of the University of Missouri - Rolla, under Contract DAAF01-69-C-0541. The investigation was performed by Dr. R. C. Tooke as partial fulfillment of the requirements for a doctoral degree.

The contract was part of a continuing gun barrel technology program authorized and funded by the U. S. Army Small Arms Systems Agency.

The work was conducted under the direction of the Research Directorate, Weapons Laboratory, Rock Island Arsenal, with Dr. W. T. Ebihara as Project Engineer.

## ABSTRACT

As a segment of a small arms program at the Research Directorate, Weapons Laboratory, Rock Island Arsenal, the erosion process in 7.62mm steel gun barrels has been chronologically characterized by investigation of the test-fired barrels fired from 1 to 3000 rounds. Both unplated barrels and barrels with hard chromium plated bores were included. Detailed metallurgical analysis, using modern analytical techniques, was conducted on the test-fired gun barrels. Evidence is presented to demonstrate that chemical effects substantially augment the erosion phenomenon caused by thermomechanical factors. Gas-metal reactions and chemical attack involving Pb, S, Cu (Cu-Zn) and Ca comprise the observed chemical effects. Although the chromium plating resists chemical attack of the underlying steel, inherent defects in the plating act as crack initiators. Cracks propagate from the plating defects into the steel moving both laterally and radially to cause removal of plating fragments and eventual rupture of the gun tube. In addition to the contribution to crack propagation, chemical effects are in evidence uniformly over the entire bore surface of unplated barrels. To complement the erosion analysis, cantilever-fatigue tests on unplated and Cr-plated Cr-Mo-V steel specimens in reactive environments at elevated temperatures were conducted. The analysis of the cracking phenomenon in reactive environments included an examination of the role of chromium plating in reducing fatigue life.

## CONTENTS

	<u>Page</u>
TITLE PAGE	i
FOREWORD	ii
ABSTRACT	iii
TABLE OF CONTENTS	iv
TABULAR DATA	vii
ILLUSTRATIONS	viii
I. PART I. EROSION ANALYSIS AND CHARACTERIZATION	1
A. INTRODUCTION	1
B. PROCEDURE	1
a. Test-Fired Barrels	1
b. Visual Examination	3
c. Metallographic Examination	3
d. Microhardness Measurements	3
e. X-ray Diffraction	3
f. Scanning Electron Microscopy	4
g. Electron Microprobe and Nondispersive X-ray Analyses	4
C. RESULTS	5
a. Visual Examination	5

## CONTENTS (Continued)

	<u>Page</u>
b. Microhardness Tests	5
c. X-ray Analysis	5
d. Microscopic and Analytical Results	7
1. Chromium Plated Barrels	7
2. Unplated Barrels	12
3. Advanced Stages of Erosion	13
D. DISCUSSION OF RESULTS	15
E. PART I SUMMARY	19
II. PART II. FATIGUE BEHAVIOR IN REACTIVE ENVIRONMENTS	61
A. INTRODUCTION	61
B. EXPERIMENTAL PROCEDURE	62
a. Apparatus	62
b. Specimen Preparation and Test Procedure	65
C. RESULTS	66
D. DISCUSSION OF RESULTS	70
E. PART II SUMMARY	73
LITERATURE CITED	98
APPENDICES	
A. Results of Visual Inspection of Test-Fired Barrels	101

## CONTENTS (Continued)

	<u>Page</u>
B. X-ray Diffraction Data	104
C. Normalized and Actual Intensities	105
D. Combustion Gas Composition and Sample Calculation	107
DISTRIBUTION	109
DD FORM 1473 (Document Control Data - R&D)	113

## TABULAR DATA

<u>Table</u>		<u>Page</u>
I	Test-Fired Barrels	2
II	Microhardness Results	6
III	Metallographic Observations on Barrel C-200	10
IV	Metallographic Observations on Barrel C-3000	11
V	Experimental Fatigue Data	67

## ILLUSTRATIONS

<u>Figure</u>		<u>Page</u>
1	Standard for nondispersive X-ray spectrometer used with scanning electron microscope for chemical identification.	21
2	Inherent defects in chromium plating.	22
3	Pits developing in steel at base of cracks in Cr plating. Barrel C-10.	23
4	Results of X-ray spectrometer analysis of pit in barrel C-50.	24
5	Propagation of cracks in Cr plating into steel. Barrel C-100, bore surface sample, unetched, 250X.	25
6	Chemical analysis of bore surface of barrel C-100.	25
7	Photomicrographs of pits and cracks in barrel C-200.	26
8	Scanning electron micrographs depicting the presence of fine intergranular cracks (top) and crack-pit combinations (bottom). Barrel C-200A, nital etch. 3000X.	27
9	Chemical analysis of area indicated by white dot in pit of top photograph. Barrel C-200.	28
10	Chemical analysis in crack leading from pit at location indicated by white dot in top photograph. Barrel C-200.	29
11	Cracks and reaction zone typical of barrel C-661.	30

## ILLUSTRATIONS (Continued)

<u>Figure</u>		<u>Page</u>
12	Chemical analysis of crack in barrel C-900. Area of analysis indicated by black dot in top photograph.	31
13	Removal of Cr plating grain. Scanning electron micrograph, barrel C-900, transverse section. Unetched, 1000X.	32
14	Chemical analysis of crack (white dot) in barrel C-2100. Analysis in reaction zone (black dot - not shown) yielded no foreign elements.	33
15	Scanning electron micrographs of hole left in bore of barrel C-2100 after Cr removal. Top-300X, Bottom-1000X.	34
16	Chemical analysis of crack at area indicated by black dot in top photograph. Barrel C-3000.	35
17	Photomicrographs of the condition of cracking representative of barrel C-3000.	36
18	Scanning electron micrograph of reaction zone formation characteristic of areas 5-10 inches from origin of rifling in barrel C-3000. Transverse sample, nital etch, 3000X.	37
19	Crack progression in Cr plated barrels. Transverse samples, 100X. Top C-900, Middle C-1500, Bottom C-3000.	38
20	Photomicrographs of unplated barrels at the beginning of test firing.	39

## ILLUSTRATIONS (Continued)

<u>Figure</u>		<u>Page</u>
21	Scanning electron micrographs of crust on bore surface of barrel U-300.	40
22	Chemical analysis representative of bore surface of barrel U-300.	41
23	Cracking in barrel U-661.	42
24	General attack resembling reaction zone over entire surface of bore of barrel U-661. Unetched, 500X.	43
25	Scanning electron micrographs of attack on barrel U-900. Bore surface sample.	44
26	Chemical analysis of position 2 identified in Figure 25(b). Position 1 analyzed similar to 2; position 3 the same as base steel.	45
27	Scanning electron micrographs of bore surface topology, barrel U-3000.	46
28	Photomicrographs of crack network in barrel U-3000.	47
29	Photomicrographs of the reaction zone in barrel U-3000.	48
30	Chemical analysis of bore surface of barrel U-3000 (Figure 27).	49
31	Chemical analysis of crack and reaction zone in barrel U-3000.	50

## ILLUSTRATIONS (Continued)

<u>Figure</u>		<u>Page</u>
32	Electron microprobe results from crack in barrel U-3000. 500X.	51
33	Crack progression in unplated barrels. Transverse samples, 100X. Top U-900, Middle U-1500, Bottom U-3000.	52
34	Copper deposits in incoherent Cr plating.	53
35	Reaction zone in severely eroded barrels.	54
36	Microhardness test (25 gram load). Knoop hardness numbers shown. 250X.	55
37	Chemical analysis of Cu-filled crack and reaction zone in severely eroded barrel.	56
38	Chemical analysis of crack and reaction zone in severely eroded barrel.	57
39	Electron microprobe analysis by back-scattered electrons of crack network with reaction zone in severely eroded barrel. 500X.	58
40	Electron microprobe analysis of crack and reaction zone in severely eroded barrel. 1000X.	59
41	Electron microprobe analysis of a hemispherical shaped reaction zone in the steel at the base of an existing crack in chromium plating. 1000X.	60
42	Catastrophic failure in 7.62mm gun barrel.	74

## ILLUSTRATIONS (Continued)

<u>Figure</u>		<u>Page</u>
43	Reactions of iron with CO/CO <sub>2</sub> atmospheres. <sup>5</sup>	75
44	Photograph of apparatus.	76
45	Diagram of apparatus components.	77
46	Test chamber.	78
47	Induction coil with specimen at 1000C.	79
48	Temperature profiles in specimen heated in induction coil.	80
49	Temperature calibration curve.	81
50	Test specimen dimensions.	82
51	Gage section of test specimens: right, unplated; left, Cr plated.	83
52	Test specimens after failure: right, unplated; left, Cr plated.	83
53	Plot of fatigue life as a function of gas composition.	84
54	Pitting beneath Cr plating typical of high CO <sub>2</sub> mixtures. 200X.	85
55	Oxide-filled crack generating from a pit in unplated sample. 100X.	85

## ILLUSTRATIONS (Continued)

<u>Figure</u>		<u>Page</u>
56	Photomicrograph of crack representative of high CO <sub>2</sub> specimens. Nital etch. 500X.	86
57	Scanning electron micrograph of oxide in crack and mottled zone. 80% CO <sub>2</sub> . 3000X.	86
58	Crack propagation in the absence of pitting in Cr plated specimen. 500X. 50% CO <sub>2</sub> .	87
59	Crack propagation in the absence of pitting in Cr plated specimen. 200X. 50% CO <sub>2</sub> .	87
60	Mottled zone on surface of 20% CO <sub>2</sub> specimen. Unplated specimen. 500X.	88
61	Intergranular formation of precipitate in mottled zone formed at crack tip. 750X.	88
62	Fine crack in 100% CO specimen. 500X.	89
63	Altered zone around crack in 100% CO specimen. Nital etch. 500X.	89
64	Scanning electron micrograph of mottled zone. Note crack following intergranular particles. 3000X.	90
65	Scanning electron micrograph of mottled zone. Note cracking in the particles. 3000X.	90
66	X-ray spectrometer analysis of precipitate particles in mottled zone.	91

## ILLUSTRATIONS (Continued)

<u>Figure</u>		<u>Page</u>
67	Electron microprobe results of the mottled zone. 375X.	92
68	Blunt cracks in Cr-plated specimen tested in argon. 200X.	93
69	Diffusion zones formed in the Cr-plated samples. Nital etch. 500X.	93
70	Scanning electron micrograph of fracture surface topology. 20% CO <sub>2</sub> . 300X.	94
71	Scanning electron micrograph of copper film over fracture surface. 600X.	95
72	Photomicrograph of liquid Cu penetration which led to rapid failure. Penetration perpendicular to surface of specimen. 150X.	95
73	Representation of internal oxidation.	96
74	Criteria for liquid metal penetration at grain boundaries.	97

## PART I. EROSION ANALYSIS AND CHARACTERIZATION

### A. INTRODUCTION

The erosion or deterioration of the bore surface as a result of the severe conditions existing in the interior of a gun barrel remains a critical factor in limiting barrel life. Although considerable attention has been devoted to studies concerning erosion, the basic mechanisms by which progressive damage to the bore surface occurs have not been established. This erosion process is undoubtedly complex and results from a combination of events, and strongly depends on such variables as propellant chemistry, firing schedule, bore surface treatments, and barrel material. In addition, gun barrel erosion is immune to a generic interpretation because of the varying erosion processes which occur in the different weapons systems.

Erosion tests usually concern effects such as decrease in projectile velocity, flight stability, and accuracy rather than causes of damage to the gun barrel. The present investigation represents a metallurgical approach to the investigation of erosion in small caliber gun barrels in which analytical equipment, only recently commercially available, was used. The test apparatus involved is the 7.62mm Minigun. This study, primarily analytical in nature, chronologically defines the physical and chemical changes which occur in systematically test-fired barrels. The information contained herein is necessary for the understanding of the erosion problem in small caliber weapons and, therefore, contributes to the general erosion investigation program being conducted at the Research Directorate, Weapons Laboratory, RIA.

### B. PROCEDURE

#### a. Test-Fired Barrels:

A progressive firing program was developed; 7.62mm gun barrels, in the unplated condition and with hard chromium plated bores, were subjected to this program according to the schedules of Table I. Each barrel was fired as part of a six barrel complement on the GAU-2B/A Minigun weapon. In all cases, the rate of firing was 4000 rounds per minute or approximately 667 rounds per minute per barrel. The ammunition consisted of 7.62mm, NATO, Ball, M80 with propellant WC846, lot TWL-18068-67 (up through barrel U-661) and lot TWL-18337-69.

TABLE I  
TEST-FIRED BARRELS

<u>Barrel Identification</u>	<u>Description</u>	<u>Rounds Fired</u>	<u>Schedule (per 6 barrel complement)</u>
C-1	Cr plated	1	Continuous burst at 4000 rounds per minute
C-10	Cr plated	10	
C-50	Cr plated	50	
C-100	Cr plated	100	
C-200	Cr plated	200	
U-1	unplated	1	
U-10	unplated	10	
U-50	unplated	50	
U-100	unplated	100	
U-200	unplated	200	
C-300	Cr plated	300	600-round bursts at 4000 rounds per minute with 15-second cooling between each burst
U-300	unplated	300	
C-661	Cr plated	661	Composite of above two schedules
U-661	unplated	661	
C-900	Cr plated	900	Three 600-round bursts at 4000 rounds per minute with 15-second cooling between each burst. Repeat following complete cool down
C-1500	Cr plated	1500	
C-2100	Cr plated	2100	
C-3000	Cr plated	3000	
U-900	unplated	900	
U-1500	unplated	1500	
U-2100	unplated	2100	
U-3000	unplated	3000	

In addition to the above-described barrels, several severely eroded Cr-plated barrels, which had been fired extensively under a separate contract,<sup>1</sup> were procured for investigation.

b. Visual Examination:

Initially, silicone replicas were made which allowed nondestructive examination of the interior bore surface. Further macroexamination was considered imperative; therefore, the gun barrels were halved longitudinally which made the inspection of the bore surface possible. Inspection was done by both the unaided eye and at low magnification (40X) with the assistance of a binocular microscope.

c. Metallographic Examination:

Optical metallography was performed on samples obtained from each of the gun barrels. The majority of the samples were taken from the first four inches (from origin of rifling) of the barrel because experience has shown this to be the region of the bore which is most damaged. Two types of specimens were prepared for studying barrel damage -- a transverse specimen and a specimen polished at a low angle to the bore surface and referred to as a bore surface specimen. The bore surface specimens were necessary to enable viewing of barrel damage even though the damage did not extend to any appreciable depth and could not be satisfactorily observed on a transverse section.

Occasionally, nickel plating was incorporated to assist in edge retention at the bore surface. All samples were mounted in Bakelite. Standard polishing procedures were followed with 6 $\mu$  and 1 $\mu$  diamond and .05 $\mu$  alumina abrasives. Before analysis, all samples were ultrasonically cleaned to ensure removal of polishing residues. Metallographic specimens were observed in the unetched and etched condition, a 5% nital etch being the most common. Magnifications ranged from 100X to 1000X.

d. Microhardness Measurements:

Microhardness tests were made with a Knoop indenter at loads of 25 grams and 100 grams.

e. X-ray Diffraction:

Powder samples for X-ray diffraction analyses were obtained by scraping the bore surface with a sharp object

and by filing previously prepared bore surface samples. After collection of the powder, it was placed and sealed in a .3mm diameter capillary tube. The fiber thus formed was used to obtain a diffraction pattern with a Debye-Scherrer camera ( $d = 114.6\text{mm}$ ). Copper (Ni filter) and iron (Mn filter) radiation were used with 4-8 hour exposures.

f. Scanning Electron Microscopy:

A microscopic study of the test fired barrels was made with a JEM-2 scanning electron microscope (SEM). Both polished specimens and surface samples of as-fired barrels were checked.

The attractiveness of the SEM is due primarily to a few unique features. One is the ability to observe surfaces directly at high magnifications. This was particularly useful in examinations of the as-fired bore surface. Another is the great depth of focus (about 300 times that of an optical microscope) and the three-dimensional nature of the image obtained. The resolving power of the SEM is approximately  $250\text{\AA}$ , with magnifications from 20X-50,000X. The magnification attainable is dependent upon the nature of the specimen. In this particular study, the most common range was 1000X-3000X.

When the high-energy electron beam of the SEM strikes the surface of the sample, some of the electrons are absorbed; but some cause X-rays, secondary electrons, and backscattered electrons to be emitted.

Any of these can be detected and analyzed, but with different results. The X-rays can be used for chemical analysis such as in electron microprobe techniques or with a nondispersive X-ray attachment to a conventional SEM. The backscattered electrons can give information related to the atomic number of the elements on the surface. The secondary electrons are most commonly used as they provide a greater capability of allowing observation of depressions and rough, irregular surfaces. In almost all cases, the specimen was located perpendicular to the beam.

g. Electron Microprobe and Nondispersive X-ray Analyses:

Identifications of the chemical elements associated with the eroded areas and variations in the base steel chemistry with firing schedule were made with an ARL microprobe. Standard microprobe techniques were used in all cases.

When particularly fine details and cracks were involved, chemical determinations were made with the nondispersive X-ray spectrometer attachment on the scanning electron microscope. With the SEM, it was possible to position the electron beam on any area desired. This allowed detection of elements in finely disseminated minute areas; however, these were not present in sufficient quantities to be located accurately enough to allow analysis with the microprobe.

Samples used in this phase of the work were also used in the metallographic and microscopic studies.

### C. RESULTS

#### a. Visual Examination:

Brief summaries of the observations made on each of the test-fired barrels are contained in Appendix A. In summary, the crack network in the chromium becomes obvious in the early stages of firing with eventual fragmenting, displacement, and removal of Cr-plate particles. These inherent cracks in the plating collect more copper in the breech end compared to the unplated barrels, although both plated and unplated barrels develop heavy deposits of copper in the muzzle half of the barrel. The rifling is eliminated in the first several inches of the unplated barrel after 1500 rounds, but remains sharp in the plated barrels through 3000 rounds except for deterioration by Cr particle removal. The Cr crack network is apparent after 50 rounds; however, checking of the bore surface of the unplated barrels was not observed until 900 rounds.

#### b. Microhardness Tests:

The results of microhardness tests on transverse samples are given in Table II. The purpose of these tests was to determine the extent of bore softening. The position of the indentation is the depth from the bore surface on unplated barrels and from the Cr-steel interface on plated barrels. These data indicate no significant softening in the plated barrels, but some shallow softening of the unplated barrels appears to exist.

#### c. X-ray Analysis:

Representative data resulting from X-ray diffraction

TABLE II

## MICROHARDNESS RESULTS

		Knoop Hardness Number Depth into Steel (inches)					
		<u>.001</u>	<u>.003</u>	<u>.005</u>	<u>.010</u>	<u>.015</u>	<u>.025</u>
C-661	(~1")	326	358	347			
		317	340	331	347		352
U-661	(~1")	290	341	352	358	347	336
		326					
C-2100	(~1")	320	341	352	358	352	370
C-2100	(~3")	321	358	370	365	347	358
U-2100	(~1")	267	352	347	358	370	347
U-2100	(~3")	274	317	326	326	321	
		317	330	330	352	352	
C-3000	(~1")	326	347	341	352	352	352
C-3000	(~3")	370	358	347	347	358	347
U-3000	(~1")	321	358	358	370	358	370
		317	365	377	377	370	377
U-3000	(~3")	282	352	352	358	352	352

examination are given in Appendix B. These diffraction lines were repeated in many other samples. Positive identification of  $\text{CaCO}_3$ ,  $\text{Cu}(\text{CuZn})$  and  $\text{Pb}$  was made in addition to the  $\alpha\text{-Fe}$  of the steel. On the basis of the diffraction data, either or both  $\text{Fe}_2\text{O}_3$  and  $\text{Fe}_3\text{O}_4$  are strongly believed to be present. Oxides of copper and lead may also be present.

d. Microscopic and Analytical Results:

This portion of the results will be divided into several sections. First, the results from the test-fired chromium-plated barrels will be presented followed by the results from the test-fired unplated barrels. Results which characterize the advanced stages of erosion are presented in the final section which comprises data obtained from barrels which had been subjected to severe firing schedules.

An example of the data obtained from the nondispersive X-ray spectrometer is shown in Figure 1. For initial qualitative chemical analyses, the cathode ray tube display is satisfactory; however, the printout sheet of this display is required for more detailed semiquantitative analysis. Accurate identification of peaks and relative intensity ratios included in the following results were obtained from similar printout sheets. (Refer to Appendix C).

1. Chromium Plated Barrels:

The data of Figure 1 are from the base barrel material which is the standard Cr-Mo-V steel with compositional limits as follows:

<u>Element</u>	<u>Wt. %</u>
Carbon	.41 - .49
Manganese	.60 - .90
Phosphorous	.040 max
Sulfur	.040 max
Silicon	.20 - .35
Chromium	.80 - 1.15
Molybdenum	.30 - .40
Vanadium	.20 - .30
Iron	balance

The nondispersive X-ray spectrometer is incapable of detecting elements below sodium, atomic number 11 in the Periodic Table. Occasionally spurious peaks occurred in the

spectrometer analyses which could not be identified. In addition, certain elements, namely aluminum, iron, and chromium were almost always detected due to unshielded pieces of these metals being present within the analyzing chamber. Therefore, caution must be used in the interpretation of these results.

Cracks were inherent in the hard chromium plating on the bore (Figure 2). The decomposition of the initially deposited chromium hydride is believed to be responsible for the presence of high stress in the deposit. During transformation to stable body-centered cubic chromium, a volume contraction of up to 15% takes place. The Cr layer first grows a certain thickness and then cracks form because of the high tensile stress.<sup>2</sup> The thickness of the plating was nominally 2.5 mils, and the hardness was approximately Rc 66-70. After one round, the cracks became more obvious in the plating; repeated firing continued to expand the initial cracks and also created new ones.

The first evidence of any alteration appeared at the Cr-steel interface after only ten rounds, as is shown in Figure 3. These pits were always observed to be associated with cracks in the plating, but all of the cracks did not result in pits. This pitting condition had not significantly changed after 50 rounds; however, an almost complete absence of pitting was observed on the barrel fired for 100 rounds. An X-ray spectrometer analysis of a pit in barrel C-50 (Figure 4) showed Pb, Ca, and possibly P to be present. The presence of P was also indicated in the pits in barrel C-10. Bore surface samples from barrel C-100 did show extension of cracks into the steel which is depicted in Figure 5. After 100 rounds, the chemistry of the bore surface, Figure 6, included aluminum, lead,\* sulfur,\* calcium, copper and zinc. No foreign elements were detected in the fine cracks of the C-100 barrel.

---

\*Throughout this report, the peak labeled Pb and S should be interpreted with caution because the nondispersive X-ray spectrometer does not have sufficient resolution to distinguish between these two elements. The electron microprobe is capable of resolving these two peaks and indicated the presence of both Pb and S.

Barrel C-200 was sectioned at various locations along its entire length, and descriptions of the appearance of the metallographic samples at each location can be found in Table III. Pits, cracks, and combinations of these were observed, examples of which are shown in Figures 7 and 8. The presence of foreign elements (Pb, S, Cu, Ca) located in the defects is indicated in Figures 9 and 10. The 300-round barrel did not exhibit any appreciable attack in excess of that exhibited by the 200-round barrel; however, a fine altered layer was present lining the cracks which appeared to be formed by chemical reaction, and will henceforth be referred to as the "reaction zone."

Cracking and reaction zone formation were found to be fully developed (Figure 11) in the barrel which had been subjected to 661 rounds. Well-defined cracks extending from the plating into the steel were frequently observed on the transverse sample (a) with the bore surface sample (b) giving a better view of the reaction zone.

Results obtained from barrel C-900 are shown in Figure 12. Lateral branching of the cracks was first noticed after 900 rounds. By this time, the main crack had expanded and was definitely filled with residue of the composition indicated in Figure 12(b). Note that the cracks emanating from the main stem are not open but consist entirely of the reaction zone. Portions of the Cr plating had been removed; this condition as well as that of part of the steel included in the particle removal is illustrated in Figure 13.

Cracking and associated reaction zone formation continued through 1500 rounds and appeared as shown in Figure 14 after 2100 rounds. Analysis of this fine crack surrounded by reaction zone resulted in finding the foreign elements at the very tip of the crack, but analysis in the reaction zone provided a chemistry identical to that of the base steel. Granular removal of the Cr plating resulted in cavities in the bore surface that can be seen in Figure 15.

The final Cr plated test barrel, C-3000, was sectioned at various locations along its entire length, and descriptions of the appearance of the metallographic samples at each location can be found in Table IV. Barrel C-3000 exhibited deep, open cracks with considerable branching and lateral cracking near the Cr-steel interface and, in some cases, even these cracks were open and contained foreign elements as shown by results given in Figure 16. Copper-filling the cracks is readily observed with the optical

TABLE III

## METALLOGRAPHIC OBSERVATIONS ON BARREL C-200

Distance From Origin of Rifling (Inch)	Description
0.5	Worst appearance of all the samples from this barrel. Transverse sample showed pitting or attack at Cr-steel interface, but the bore surface sample revealed both pitting and crack continuation. Part of the plating could be removed at anytime because attack at interface was continuous.
2	Very few pits -- rather, most of the Cr cracks continue as cracks in the steel. Some wider cracks in the plating continue as shallow blunt cracks in the steel.
3.5	Similar to 2-inch sample.
5.5	Bore surface sample exhibits fairly large pits. Transverse sample reveals only a few Cr cracks open at the interface -- most of these end in pits in the steel.
7.5	Mostly small pits -- few scattered large ones. Appears worse than previous sample. Copper crust visible.
13.0	Cracks in Cr much finer. Scattered small pits still noticeable. Crust and copper prominent.
17.0	Cracks in Cr plate are barely visible.
20.0	

TABLE IV

## METALLOGRAPHIC OBSERVATIONS ON BARREL C-3000

Distance From Origin of Rifling (Inch)	Description
1.0	Transverse samples show deep cracks with considerable branching. Also some cracking directly beneath plating at Cr-steel interface. Reaction zone surrounding the finer cracks, but not apparent in some of the large open cracks. Some chromium plating chipped out, others about to be removed.
3.0	Similar to 1-inch sample except not as much branching. Cracking and chromium removal slightly less severe.
5.5	Many hemispherical areas of reaction zone at the interface. Some of these areas contain a crack. Additional light cracking observed within reaction zone. A few of the cracks in rifling corners are open; the remainder are tight.
8.5	Much fewer hemispherical reaction zone areas. Virtually no cracks.
12.5	Shows a minimum of reaction zone at base of Cr cracks.
17.5	No attack evident. Cracks in plating not as open as previous samples.

microscope as is the reaction zone which is more prominent in the finer cracks. Both the progressed stage of cracking and Cr removal, and the continuing formation of new cracks at the base of the inherent defects in the plating are shown in the photograph of Figure 17. The nature of the barrel deterioration more distant from the origin of rifling is shown in Figure 18. The tense teardrop-shaped reaction zones were characteristic of the defects found in this area.

The progression of cracking as a function of the number of rounds fired is depicted in the composite photograph of Figure 19.

## 2. Unplated Barrels:

The unplated barrels were of the same chemical specifications previously given for the plated barrels. The unplated, unfired barrel is shown in Figure 20(a). Also shown in Figure 20(b) is the first observed evidence of any damage which is in the form of an isolated small crack in barrel U-200. The occurrence of small cracks in the corners of the rifling was also noticed at this stage of firing.

A view perpendicular to the bore surface of barrel U-300, Figure 21, illustrates the nature of the crust found there. The outer layer, which gives the appearance of having been fused, was partially removed; this removal exposed the pebbled roughness underneath. A typical analysis of the bore surface is shown in Figure 22. No difference between the outer crust and the substrate was detected.

After 661 rounds, the transverse sample showed wear of the rifling. Scattered cracks of minimal depth, with the reaction zone, were also observed. The bore surface sample, Figure 23, reveals the cracking as it appeared after 661 rounds. In addition to these defects, the barrel did exhibit alteration resembling the reaction zone over the entire surface as shown in Figure 24. The chemistry of the bore surface was similar to that already presented for barrel U-300.

Combining Figures 25 and 26 demonstrates the general type of attack on the bore of the unplated barrels. The chemical analysis shown in Figure 26 is representative of positions 1 and 2. Position 3 was analyzed as essentially the base steel. Cracking remained at a minimum in the U-900 barrel with reaction zone associated with these cracks observed. The rifling at this stage of firing remained visible,

but had been noticeably reduced in height.

The presence of cracking became more obvious in barrel U-1500. Also, the rifling was no longer in evidence. A transverse section, after 2100 rounds, disclosed significant cracking with limited bifurcation. Most of the cracks remained relatively fine. The reaction zone on the surface became increasingly apparent in barrels U-1500 and U-2100.

A view of the topology of the bore surface as it appeared after 3000 rounds can be seen in Figure 27 in which the severity of the checking is readily apparent. The appearance of these cracks extending into the steel is illustrated in the well-developed orthogonal crack network of Figure 28. Additional photographs of the condition of barrel U-3000 are included in Figure 29 which shows the reaction zone formed on the bore surface and lining the cracks.

Chemistry determinations of the bore surface, as it appears in Figure 30, yielded ample quantities of Cu, Pb, S and Ca. Lesser amounts of these elements were found in the actual cracks, the chemistry of which is represented in Figure 31. Microprobe analysis of a crack in the U-3000 barrel proved useful in determining the distribution of elements in the crack, and results typical of such analysis are found in Figure 32. Generally, backscattered electrons will indicate the average atomic number of the examined area; however, the top photograph of Figure 32 is included primarily to show the crack outline since the nature of the crack was such that it interfered with the interpretation of the BSE image. The indications of the X-ray scans were very definite; the intensity of the respective elemental X-rays were proportional to the amount of the element present. Carbon was also detected in the crack vicinity, but it could not be conclusively displayed. Microprobe analysis of the surface reaction zone showed that the percentage of chromium and carbon increased, while the percentage of iron decreased in the reaction zone layer.

Crack progression in the unplated barrels U-900, U-1500, and U-3000 is depicted in the composite photograph of Figure 33.

### 3. Advanced Stages of Erosion:

Continued firing of barrels past 3000 rounds will result in increased deterioration of the barrel as will be presented in the results of this supplementary section.

These results were obtained from barrels that had been subjected to severe firing schedules in a separate study,<sup>1</sup> and represent the advanced stages of erosion -- in many cases approaching the catastrophic stage.

The chromium plating became completely fragmented with heavy deposits of copper distributed throughout the cracks and holes. This is evident in Figure 34 in both the polished section (top) and the topographic photograph.

The reaction zone was predominant in these barrels. Figure 35 clearly reveals the zone to be made of two phases (one white, one gray). The delineation of the two phases was usually not as definite as in Figure 35(a), but more commonly is a porous mixture like that shown in Figure 35(b). Microhardness determinations in the reaction zone resulted in the data included in Figure 36. A load application of only 25 grams was used to ensure attainment of an indentation wholly within the reaction zone. Several other readings were taken in the reaction zone and the average Knoop Hardness was determined to be 1075, considerably harder than the base Cr-Mo-V steel. In addition, Figure 36 shows the hardness increasing with proximity to the crack and reaction zones -- this effect was not observed in all tests.

Examples of the results of the X-ray spectrometer analysis on the crack and reaction zone areas of the seriously eroded barrels are shown in Figures 37 and 38. The cracks were heavily contaminated, but the reaction zone exhibited only limited amounts and, in many cases, none of the usual foreign elements.

The results of electron microprobe analysis of the severely eroded barrels are displayed in Figures 39, 40, and 41. The average atomic number of the reaction zone is less than that of the base steel (Figure 39). The distribution of elements in the crack and reaction zone is shown in Figure 40. The results showed Ca and Cu deposits in the crack with the reaction zone having Fe depletion and an increase in C and Cr content. X-ray scans of the elements Pb, S, Mo, V, and Mn did not indicate a concentration of these elements in the vicinity of the crack or reaction zone. The reaction zone formed at the base of a crack in the chromium plating also exhibited Fe depletion and an increase in C content as illustrated in Figure 41. This was a bulb of reaction zone formed at the Cr-steel interface typical of those found in the plated barrels.

#### D. DISCUSSION OF RESULTS

This investigation has provided much evidence which identifies the significant contribution of chemical effects to the erosion of small caliber gun barrels. Foreign elements (phases) have been detected which show a direct association with the initiation and progression of the erosion process. Nearly all of these elements could be considered to be aggressive with respect to the Cr-Mo-V steel and, therefore, would be instrumental in decreasing the fracture toughness of the gun barrel steel. In addition, the steel surfaces, including the crack surfaces which were exposed to the bore environment, exhibited a zone apparently formed by chemical reaction.

In many previous studies, considerable emphasis has been placed on thermal-mechanical effects in the erosion process. This is documented in the two major volumes concerning gun barrel erosion.<sup>3,4</sup> The importance of this approach is obvious when one recalls the temperatures and pressures involved, but certainly not to the exclusion of chemical effects. The above references do contain the results of several comprehensive investigations into the chemical effects contributing to erosion; however, larger caliber weapons have received the most attention.

A distinct difference was present in the progression of events which occurred in erosion of the chromium-plated barrels compared to those leading to erosion in unplated barrels. Inherent cracks in the Cr plating opened up early in the firing sequence exposing areas of the underlying steel to the reactive environment; whereas, in the unplated barrels, the complete bore surface was unprotected and was subjected to the reactive environment uniformly.

Pits were formed at the root of some of the cracks in the chromium plating. These pits represented the first evidence of erosion and were observed after only ten rounds. Barrel C-100 exhibited unexplainable, anomalous behavior in that it contained no pits even though barrels with fewer (C-50) and more (C-200) rounds did show the pit defect. These results do indicate the need to apply statistical analysis, however. These pits did contain small amounts of Pb, S, Ca, and, in particular, a substantial amount of material tentatively identified as P was noted. Phosphorous was detected in pits in both the C-10 and C-50 barrel, but was not detected in any other location. This detection of phosphorous is puzzling and, since no source of this element except incendiary ammunition can be construed, it must be

viewed with skepticism, although it could have been contained in the steel.

The reaction zone, which appeared with continued firing, had been found to vary only slightly from the base steel composition. Microprobe analysis did indicate a slight iron depletion, the presence of increased carbon content of this zone. Furthermore, analysis by backscattered electrons showed the reaction zone to be of lower average atomic number than the steel. Only limited amounts of the foreign elements (Pb, S, Cu, Zn, Ca) in the reaction zone were detected by the X-ray spectrometer. The presence of the elements in the reaction zone was thought to be due more to entrapment rather than involvement as a basic step in the formation of the zone. That is, the reaction zone was probably formed by gas-metal reaction. Selected products of such a reaction would be carbides, oxides, nitrides, sulfides, and carbonyls. All of these products (and others) have been considered in previous attempts to define erosion mechanisms.

A typical analysis of the combustion gases from propellant WC-846 can be found in Appendix D.<sup>5</sup> Also included in Appendix D are calculations based on this gas composition which form the basis for prediction of the gas to be oxidizing and carburizing. The reaction zone resembled an oxide in appearance, but attempts to identify oxide phases analytically were inconclusive. Oxygen was not positively detected by the electron microprobe; however, X-ray diffraction of the bore surface of unplated barrels produced an extra line ( $d = 2.51$ ) which corresponds to a high intensity line of  $\text{Fe}_3\text{O}_4$  and  $\text{Fe}_2\text{O}_3$ . However, note that these products could also form under storage conditions. The reaction zone was determined to be an area of carbon concentration. Efforts to determine the quantitative analysis of the reaction zone with the microprobe yielded a composition of 2.5% carbon; however, many inconsistencies were observed. In a separate investigation,<sup>6</sup> electron diffraction of the reaction zone and crack areas yielded positive identification of the phases Cu (Cu - 10% Zn), Pb,  $\alpha$  Fe, and  $\text{Cr}_{23}\text{C}_6$ , and tentative identification of  $\text{Fe}_2\text{O}_3$  and Al.

Initiation of cracking in the chromium-plated barrels seemed to be, in some instances, connected with the formation of pits at the base of the cracks in the plating. Some cracks which did not originate from pits still emanated from the Cr cracks. Undoubtedly, the sites for cracking

in the plated barrels were those areas where cracks in the plating exist. In contrast to the plated barrels, the unplated barrels developed uniform attack and wear over the entire surface. The fact that crack initiation in the unplated barrels was delayed until approximately U-661 could be explained by considering that for plated gun tubes the existing Cr crack offered both a notch effect and a site for selective chemical attack. Further, overall wear in unplated gun barrels could be expected to remove cracks as soon as they are initiated. Even when cracking occurred, overall wear of the bore surface continued in the unplated barrels.

Once initiated, cracks propagated radially by the same mechanism in both the plated and unplated barrels. The propagation was believed to be a continuing reaction-cracking sequence synonymous with corrosion fatigue. Expanding, a chemical reaction would provide a condition more favorable for cracking under the imposed stresses; therefore, cracking would occur which exposes fresh surfaces to the aggressive environment found to be present. The progression resulting from such a mechanism would be very dependent on variables such as temperature, stress level and distribution, crack depth and width, and, of course, the environment and reaction products.

The actual reaction which exerts the most influence on the cracking is speculative. Essentially, two possibilities exist from a chemical viewpoint for the nature of the reaction which controls propagation. The first would be to assume that the reaction zone forms by gas-metal reaction and the hard brittle zone fails at the crack tip exposing new surfaces. The second would be to assume that the foreign elements induce cracking in a manner similar to liquid metal embrittlement or hot shortness. However, a recent firing test involving Fe-clad and brass-clad projectiles revealed that possible Cu-Zn embrittlement would not appear to contribute significantly to crack propagation in sections near the origin of rifling.<sup>7</sup> Such findings do not completely rule out possible liquid metal reactions in 7.62mm steel gun tube sections near the muzzle end. A multitude of sequential combinations involving these two mechanisms could also be envisioned.

Of the foreign elements detected in the cracks, Pb, S, Cu, and their compounds will significantly attack steel. At the tip of the crack, Pb, S, and Ca seemed to predominate with the relative amount of Cu increasing as the main stem of the crack was approached. Calcium, if present as  $\text{CaCO}_3$ ,

would be considered to be an inert residue. Other forms such as  $\text{CaO}$  might conceivably act as a flux. Aluminum, which was always detected, is of no significance since it came from microscope parts or, perhaps, the polishing compound ( $\text{Al}_2\text{O}_3$ ). The source of these foreign elements is as follows: Cu, Zn -- projectile; Pb -- primer, propellant, projectile; S -- primer;  $\text{CaCO}_3$  -- propellant.

With continued firing, the cracks widen and lateral branching began at approximately 900 rounds; this condition was magnified through 3000 rounds. This branching resulted in undermining of the chromium layer (including some steel) with subsequent removal of particles from the bore surface. A similar type of removal of steel particles occurred to a lesser extent in the unplated barrels. Not only did the existing cracks grow under repeated firing, but new cracks and teardrop-shaped reaction zones were observed to form especially in the chromium-plated barrels. Once the barrel erosion had advanced to the point represented by barrels C-3000 and U-3000, further firing would only result in more severe stages of the conditions already described. The cracks after 3000 rounds were thought to be approaching the depth at which catastrophic failure was imminent.

The hard chromium plating satisfactorily resists both wear and chemical attack. Unfortunately the inherent cracks provide a path for deterioration of the steel substrate. If an intermediate layer between the chromium and the steel could be developed to resist chemical attack and subsequent crack propagation, the barrel life could be appreciably extended.

Some of the analytical difficulties experienced in attempting to identify the chemical reactions which are most important in the erosion mechanism are appropriately discussed. The limited amount of material in the reaction zone imposes obvious restrictions. In conjunction with this, the accurate analytical determination of low atomic number elements such as oxygen, nitrogen, and even carbon is difficult at best. Furthermore, the topographies of the areas analyzed with the nondispersive X-ray spectrometer were not desirable for maximum sensitivity to qualitative determinations and, particularly, quantitative analysis.

Because of the Part I findings emphasizing the critical role played by chemical reactivity in 7.62mm gun tube erosion, the effect of various components of the environment on crack initiation and propagation in Cr-Mo-V steels was studied in Part II. An apparatus had been designed to incorporate the

variables of temperature, stress, and environment into the laboratory testing of this steel. The laboratory tests were designed to complement the reported results of Part I in establishing the erosion mechanism or defining more specifically the role the chemical environment plays in this mechanism. The results of these tests are reported in Part II of this report.

#### E. PART I SUMMARY

1. Definite evidence of chemical attack and alteration was found in connection with the erosion of 7.62mm Cr-Mo-V steel gun barrels.
2. Lead, sulfur, copper, zinc and calcium were detected in intimate contact with the eroded areas.
3. A reaction zone was found on the steel surfaces exposed to the bore environment.
4. The reaction zone is characterized by high hardness, slight Fe depletion and increased C content.
5. Only the unplated barrels exhibited any appreciable softening which could be attributed to direct exposure to the hot gases.
6. Inherent defects in the Cr plate serve as sites for crack initiation in the steel.
7. Selective chemical attack of the steel occurs at the base of cracks in the Cr plate.
8. Overall bore enlargement including elimination of the rifling resulting from uniform chemical attack and wear is in evidence in the unplated barrels.
9. Although the hard chromium plating is resistant to chemical attack and wear, superior resistance to erosion by chemical attack would result if an impervious chromium layer could be obtained.
10. Crack initiation is delayed in the unplated barrels compared to the plated barrels, but propagation occurs in a similar manner.

11. The sequence of events in the erosion of chromium plated steel gun barrels is as follows:

- (a) Pits develop at the Cr-steel interface at the base of cracks in the plating.
- (b) Cracks emanate either from pits or from existing cracks in the plating with foreign elements being detected in these areas.
- (c) Cracks continue to grow with the appearance of a reaction zone and the presence of foreign elements
- (d) Crack branching occurs which results in the removal of the protective Cr plating.

12. The sequence of events in the erosion of unplated barrels is as follows:

- (a) Uniform chemical attack results in a reaction layer over the entire surface.
- (b) The depth of rifling is decreased and eventually eliminated early in the firing sequence.
- (c) Cracks are initiated with favored locations being the corners in the rifling.
- (d) Cracks propagate as described in 11.

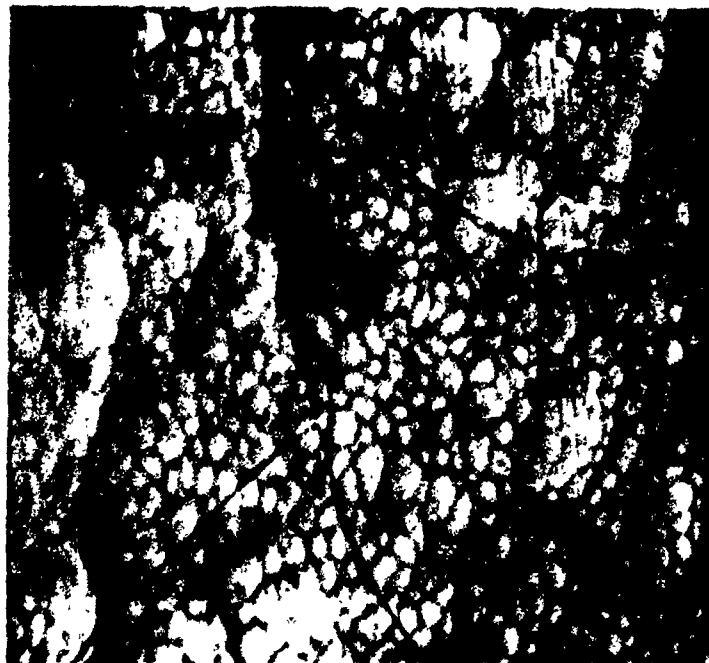


a. Cathode ray tube display

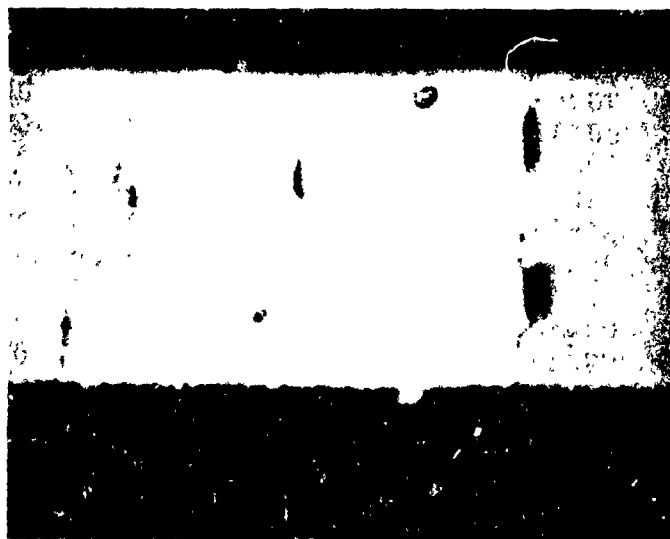
.....	.....	.....	.....	000394	000421	000443	000444
000396	000394	000431	000400	000412	000362	000419	000439
000402	000426	000393	000431	000413	000453	000457	000416
000452	000421	000411	000414	000365	000405	000441	000428
000459	000443	000499	000491	000504	000523	000491	000494
000426	000456	000430	000444	000472	000454	000502	000458
000556	000495	000510	000482	000460	000491	000452	000474
000399	000429	000472	000443	000418	000465	000504	000500
000557	000687	000747	000819	000855	000907	000916	000853
000766	000673	000637	000580	000507	000472	000486	000451
000460	000432	000478	000414	000534	000521	000579	000566
000641	000690	000696	000655	000702	000612	000585	000537
000522	000481	000500	000539	000652	000963	001368	002326
003726	005904	008722	012362	015932	019473	021597	022361
020957	018860	015424	011963	008877	006320	004431	003137
002407	001978	001591	001389	001199	001103	000935	000897
000866	000783	000806	000930	001115	001410	001785	002264
002557	002976	003287	003330	003073	002585	002118	001695
001298	000915	000711	000550	000389	000355	000328	000287
000294	000284	000221	000229	000218	000224	000198	000190
000165	000188	000183	000165	000161	000180	000176	000194
000182	000165	000167	000168	000184	000165	000175	000171
000206	000182	000172	000170	000186	000204	000188	000175
000182	000179	000176	000174	000180	000170	000146	000161
000202	000160	000168	000180	000161	000164	000150	000164
000160	000189	000177	000164	000170	.....	.....	.....

b. Portion of printout sheet (counts/channel)

Figure 1. Example of standard for non-dispersive X-ray spectrometer used with scanning electron microscope for chemical identification.

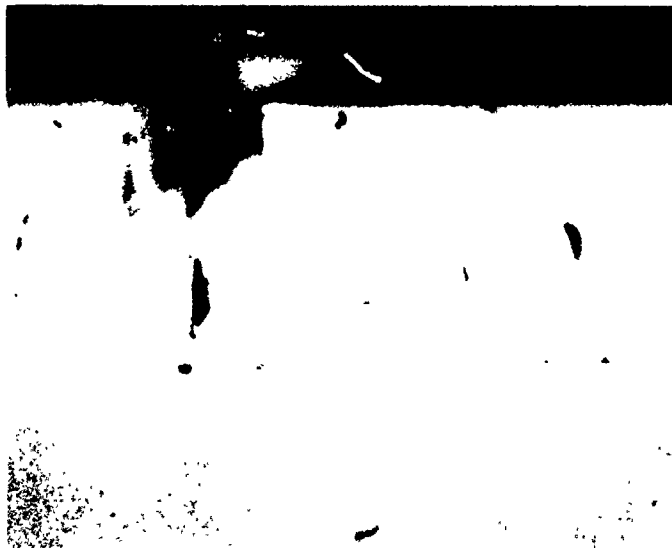


(a) Scanning electron micrograph of bore surface. Cr plated, unfired barrel. 1000X.



(b) Photomicrograph of Cr plating on unfired barrel. Etched - 4% nital, 500X.

FIGURE 2. Inherent defects in chromium plating.



(a) Photomicrograph, transverse section. Unetched, 500X.



(b) Scanning electron micrograph. Nital etch. 10,000X.

FIGURE 3. Pits developing in steel at base of cracks in Cr plating. Barrel C-10.



FIGURE 4. Results of X-ray spectrometer analysis  
of pit in barrel C-50.



FIGURE 5. Propagation of cracks in Cr plating into steel. Barrel C-100, bore surface sample, unetched, 250X.



FIGURE 6. Chemical analysis of bore surface of barrel C-100.



(a) Transverse section, nitrid etch, 250X.



(b) Bore surface sample, unetched, 1200X.

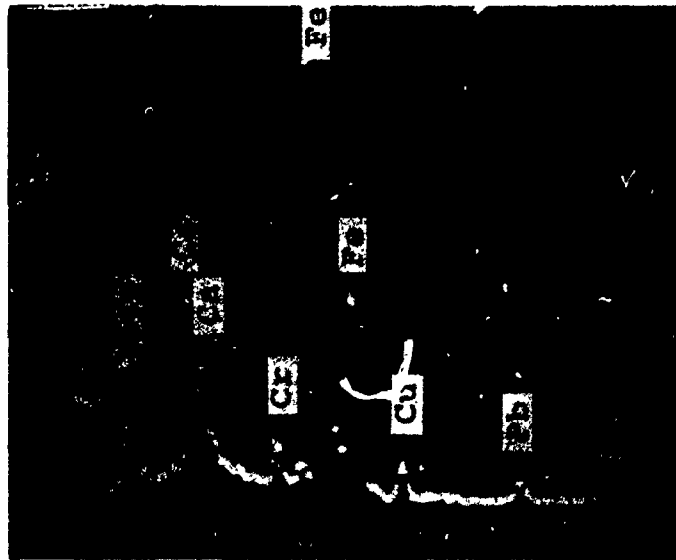
FIGURE 7. Photomicrographs of barrel C-200 showing pits and cracks.



FIGURE 8. Scanning electron micrographs depicting the presence of fine intergranular cracks (top) and crack-pit combinations (bottom). Barrel C-200A, nital etch. 3000X.



(a) Scanning electron micrograph of bore surface sample near origin of rifling. Unetched, 1000X.

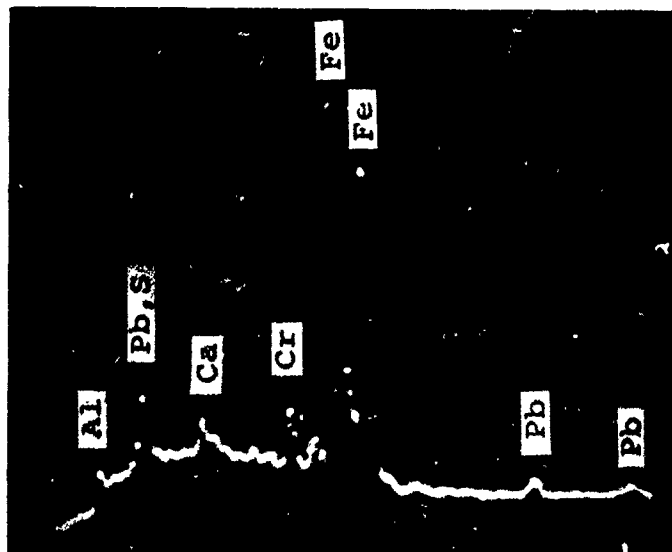


(b) X-ray spectrometer results.

FIGURE 9. Chemical analysis of area indicated by white dot in pit of top photograph. Barrel C-200.

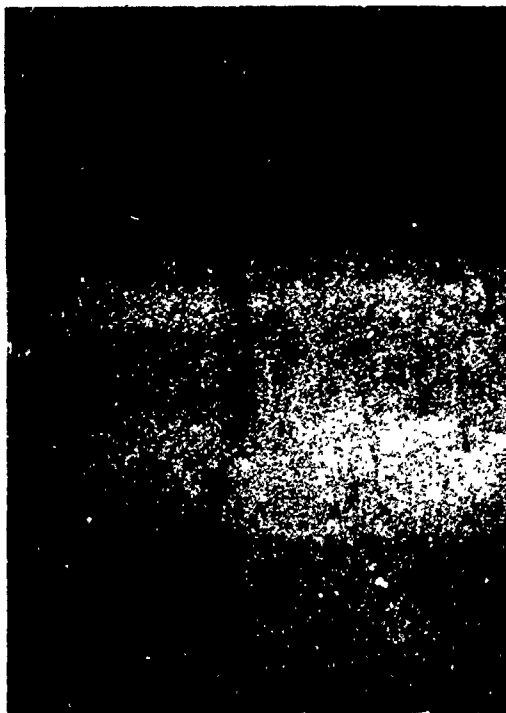


(a) Scanning electron micrograph of bore surface sample. Nital etch, 3000X.



(b) X-ray spectrometer results.

FIGURE 10. Chemical analysis in crack leading from pit at location indicated by white dot in top photograph. Barrel C-200.

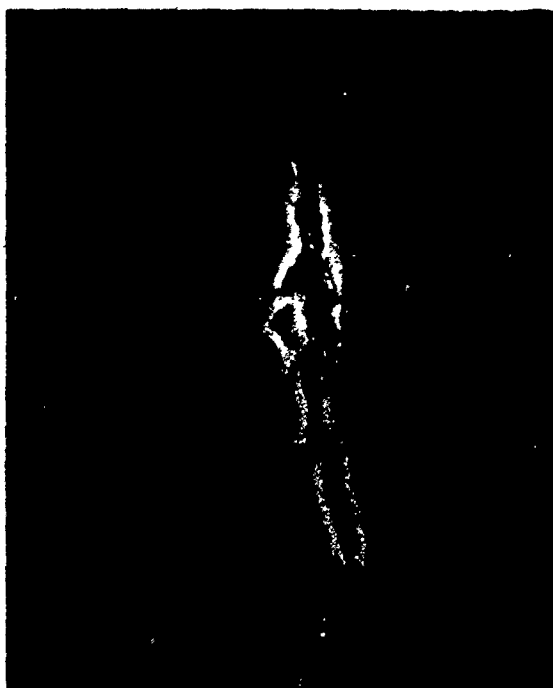


(a) Photomicrograph of transverse section.  
Unetched, 500X.

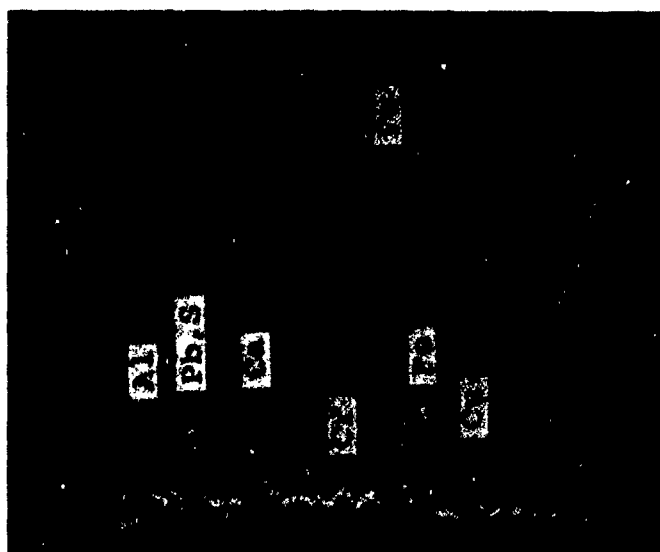


(b) Scanning electron micrograph of bore  
surface sample. Unetched, 1800X.

FIGURE 11. Cracks and reaction zone  
typical of barrel C-661.



(a) Scanning electron micrograph showing branching from main crack. Transverse section, unetched, 1000X.



(b) X-ray spectrometer results.

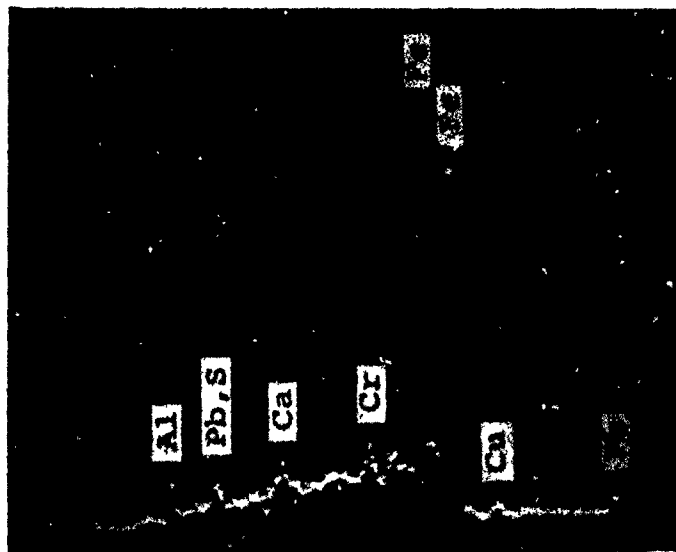
FIGURE 12. Chemical analysis of crack in barrel C-900.  
Area of analysis indicated by black dot in top photograph.



FIGURE 13. Removal of Cr plating grain. Scanning electron micrograph, barrel C-900, transverse section. Unetched, 1000X.



(a) Branch crack and reaction zone as it appeared in transverse sample. Scanning electron micrograph, unetched 3000X.

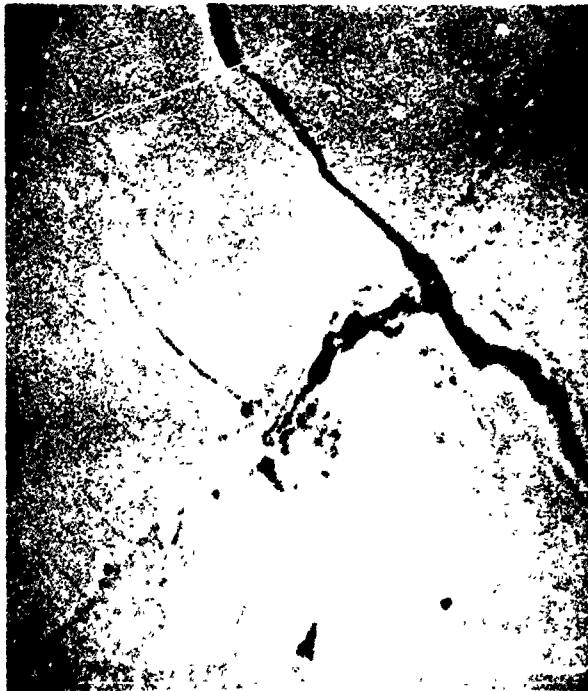


(b) X-ray spectrometer analysis.

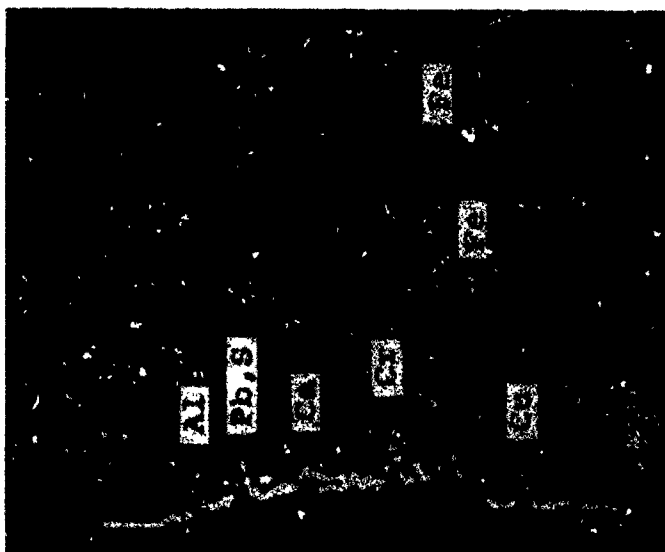
FIGURE 14. Chemical analysis of crack (white dot) in barrel C-2100. Analysis in reaction zone (black dot -- not shown) yielded no foreign elements.



FIGURE 15. Scanning electron micrographs of hole left  
in bore of barrel C-2100 after Cr removal.  
Top-300X, Bottom-1000X.

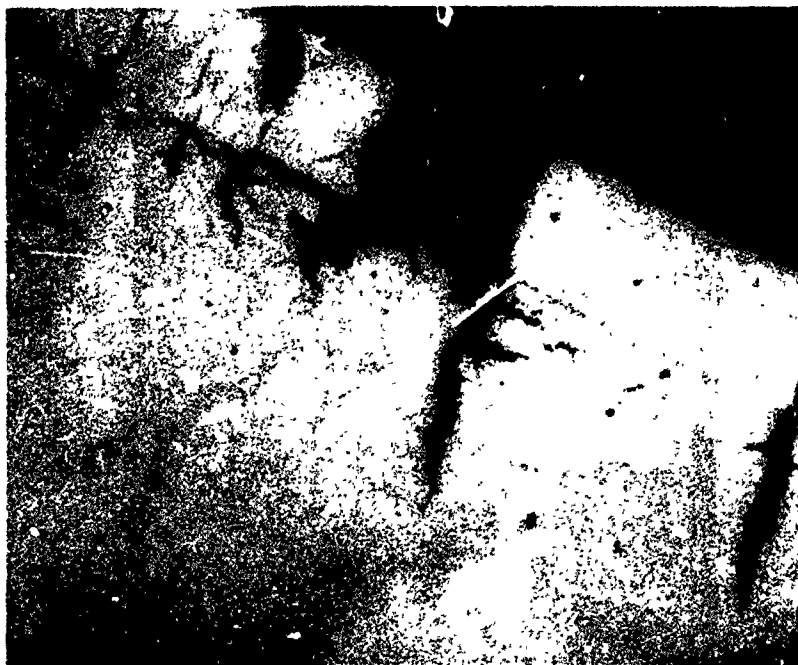


(a) Scanning electron micrograph of transverse sample. Unetched, 1000X.

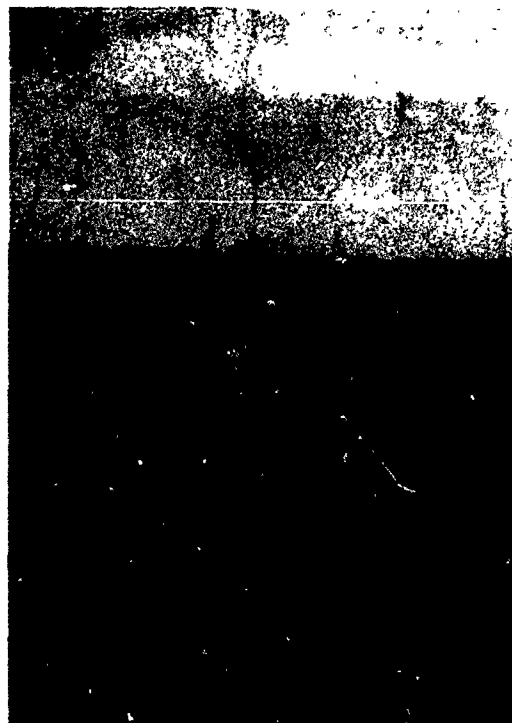


(b) X-ray spectrometer results.

FIGURE 16. Chemical analysis of crack at area indicated by black dot in top photograph. Barrel C-3000.



(a) Poor condition evident on transverse section. Unetched, 250X.



(b) Crack in early stages of formation. Transverse section, nital etch, 1000X.

FIGURE 17. Photomicrographs capturing the condition of cracking representative of barrel C-3000.

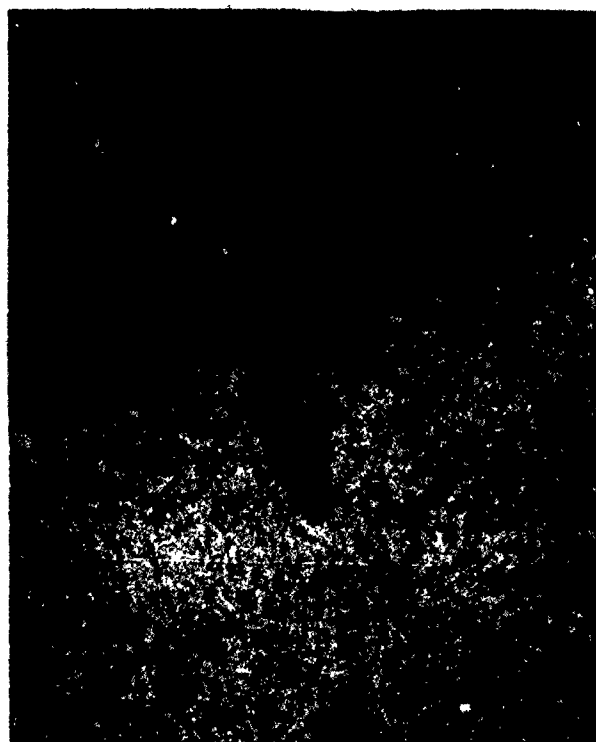


FIGURE 18. Scanning electron micrograph of reaction zone formation characteristic of areas 5-10 inches from origin of rifling in barrel C-3000. Transverse sample, nital etch, 3000X.

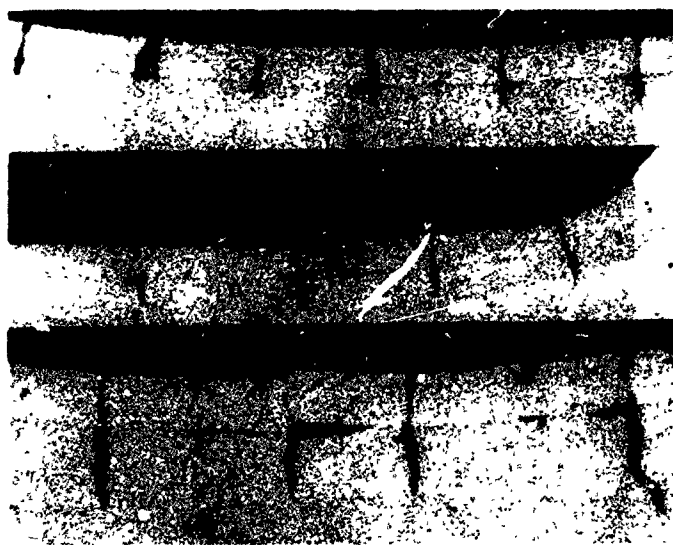
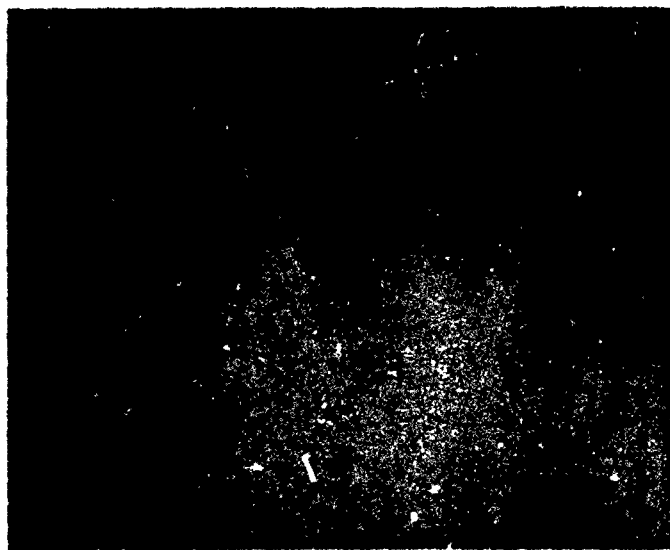
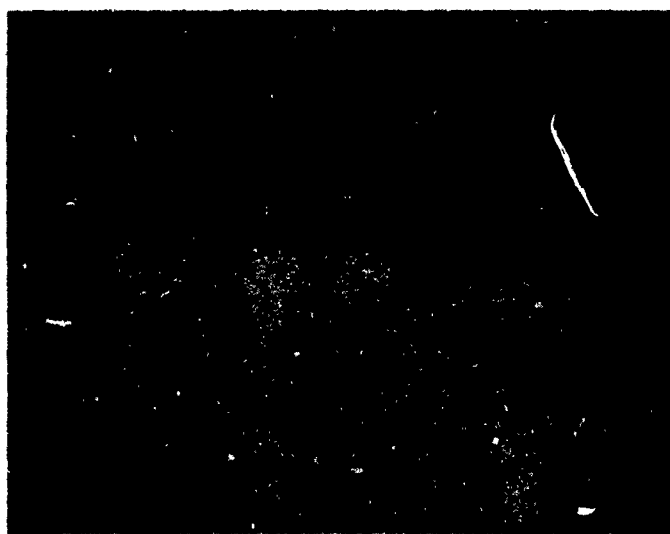


FIGURE 19. Crack progression in Cr plated barrels.  
Transverse samples, 100X. Top C-900,  
Middle C-1500, Bottom C-3000.



(a) Unfired barrel, transverse section.  
Unetched, 500X.

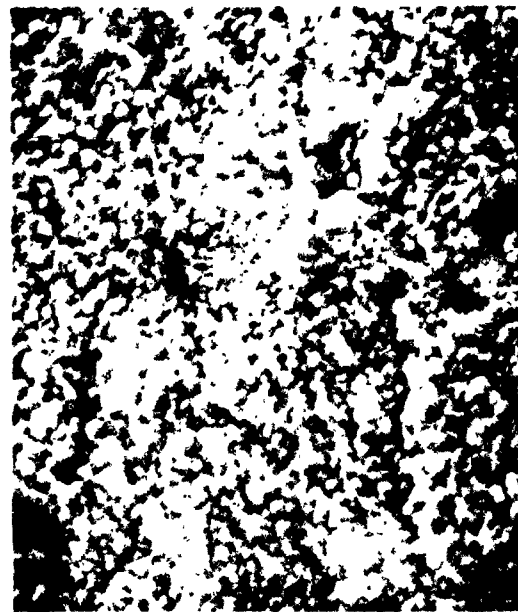


(b) Isolated crack in barrel U-200.  
Transverse section, unetched, 500X.

FIGURE 20. Photomicrographs of unplated barrels  
at the beginning of test firing.



(a) 1000X. Note fused appearance of outer layer.



(b) Left - same as (a) except 5000X. Right - closeup of substrate 3000X.

FIGURE 21. Scanning electron micrographs of crust on bore surface of barrel U-300.

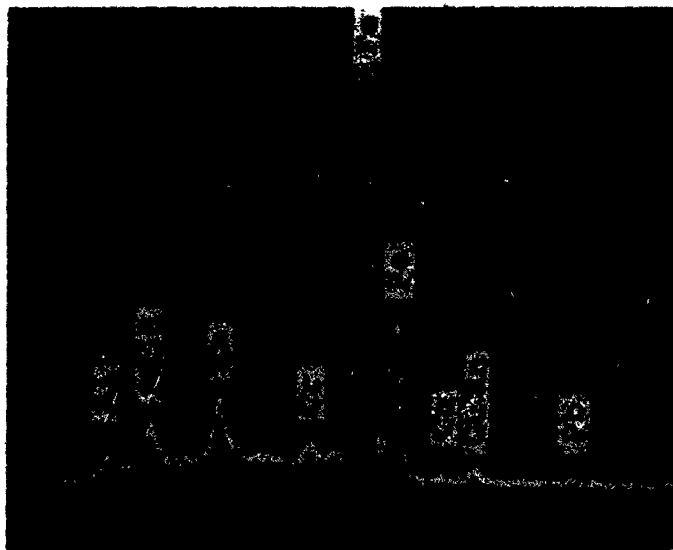
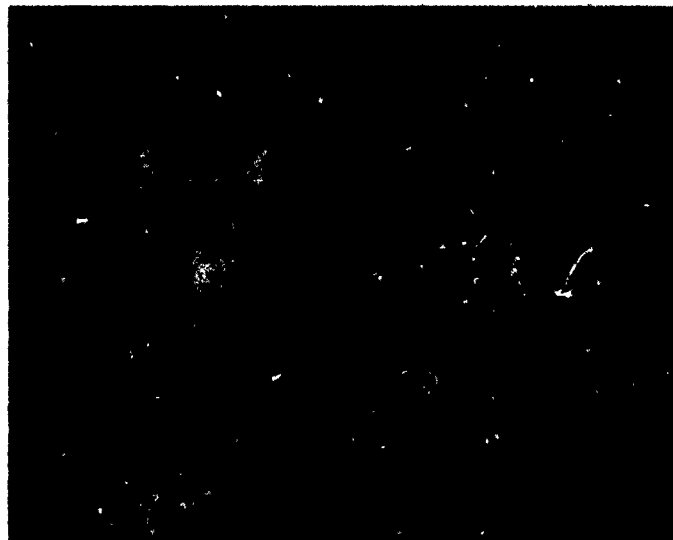


FIGURE 22. Chemical analysis representative  
of bore surface of barrel U-300.



(a) Bore surface sample, unetched, 500X.



(b) Fine intergranular cracks, revealed by nital etch. Bore surface sample, 500X.

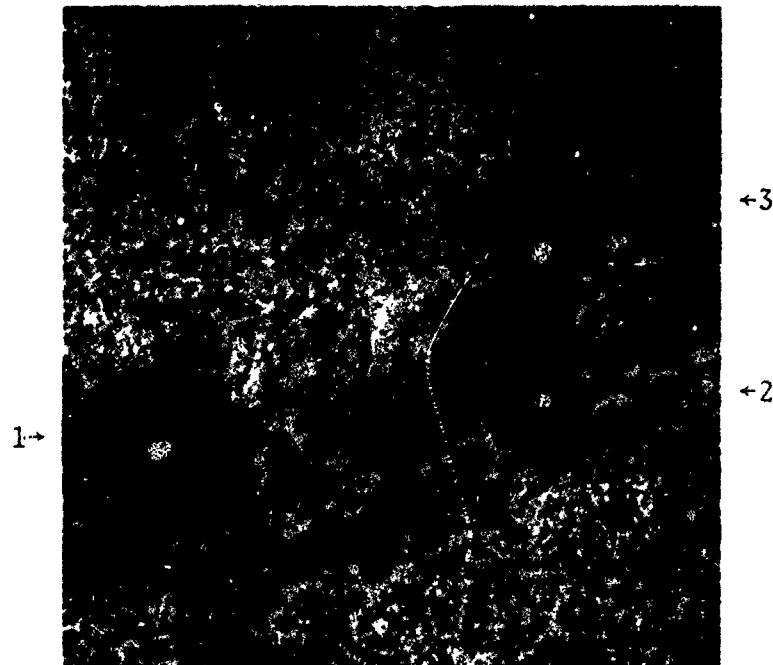
FIGURE 23. Cracking in barrel U-661.



FIGURE 24. General attack resembling reaction zone over entire surface of bore of barrel U-661. Unetched, 500X.



(a) 300X.



(b) Area of (a) at 3000X. Chemical analysis in Figure 26.

FIGURE 25. Scanning electron micrographs depicting attack on barrel U-900. Bore surface sample.

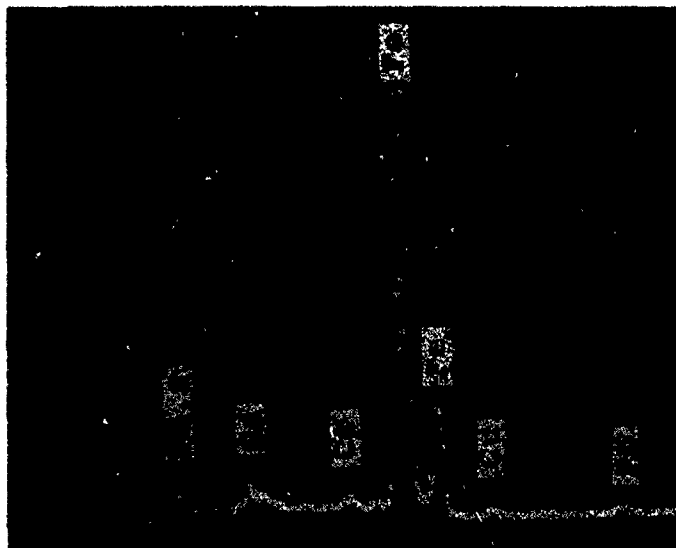
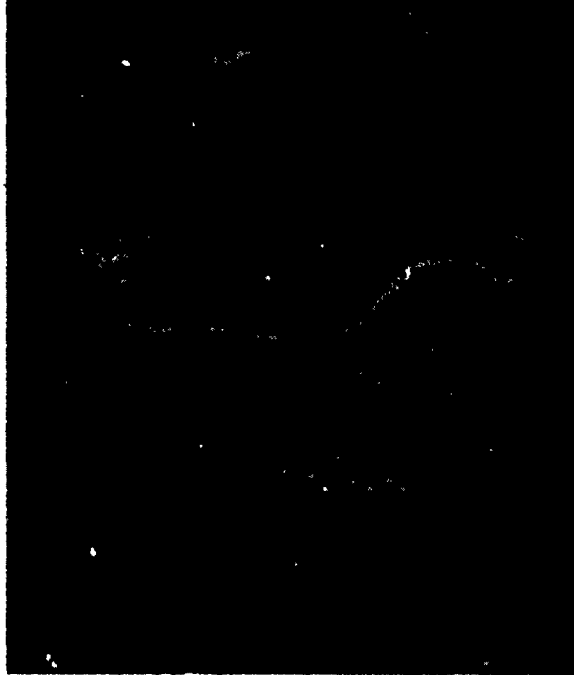
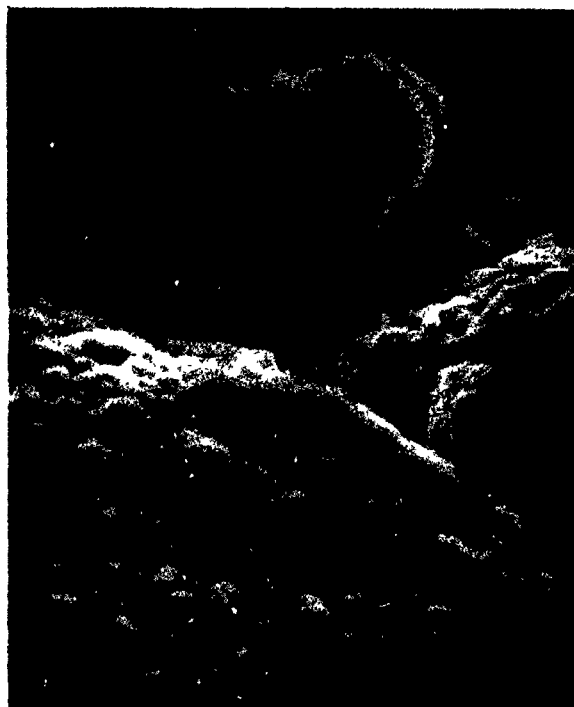


FIGURE 26. Chemical analysis of position 2 identified in Figure 25(b). Position 1 analyzed similar to 2, position 3 the same as base steel.

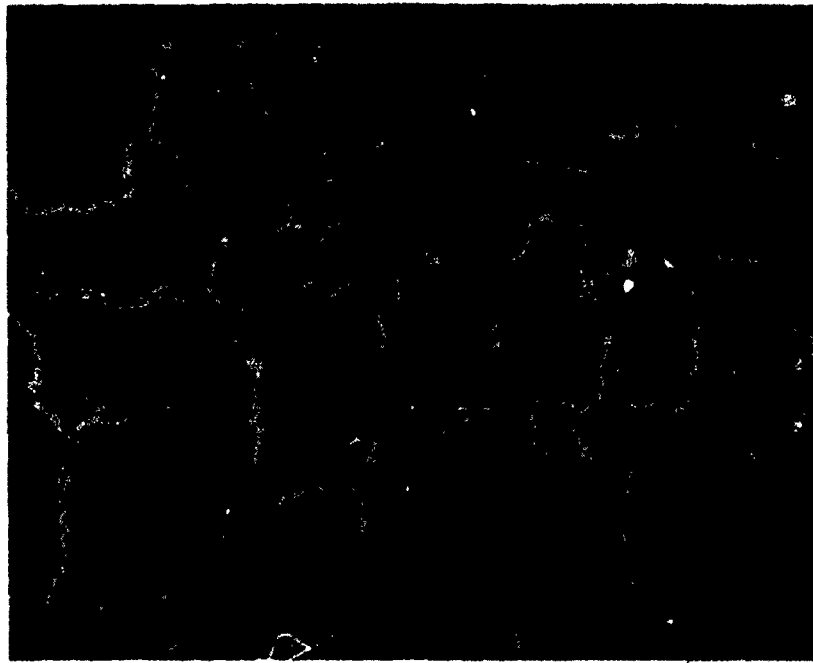


(a) "Checking" at 300X.

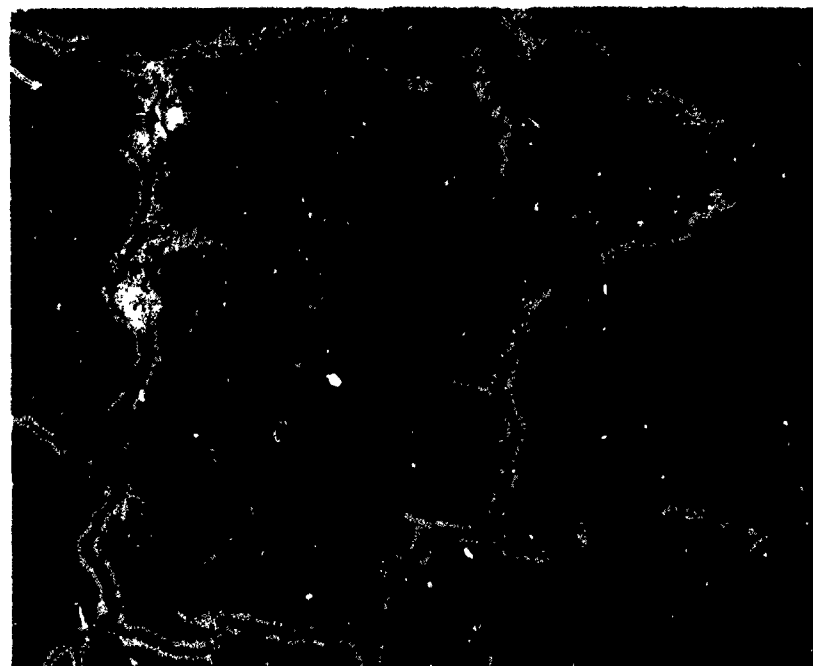


(b) Area (a) at 3000X.

FIGURE 27. Scanning electron micrographs of bore surface topology, barrel U-3000.



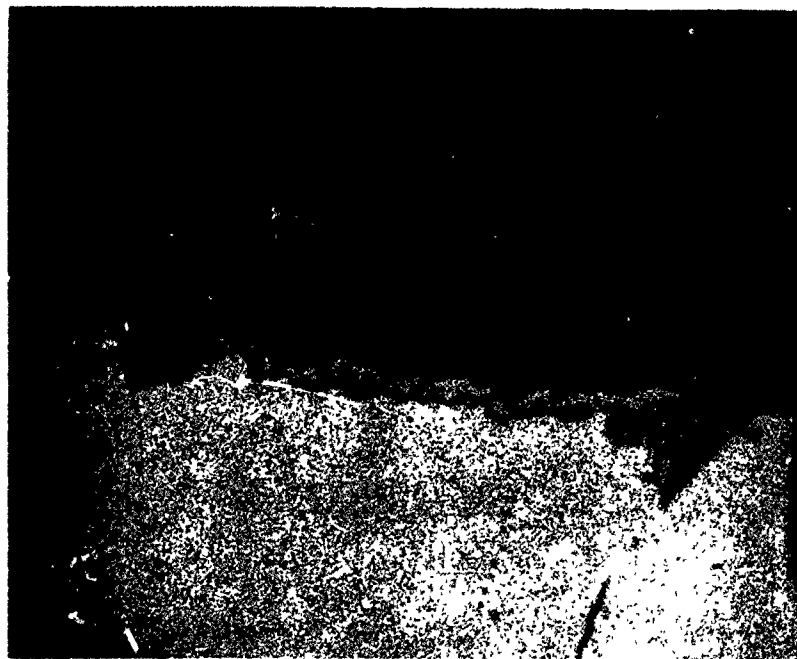
(a) Bore surface sample, nital etch, 100X.



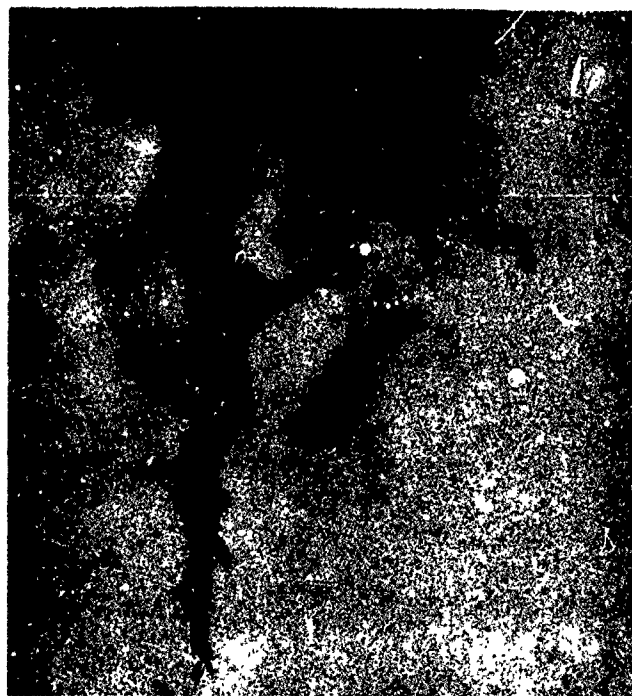
(b) Same as above, 250X.

FIGURE 28. Photomicrographs of crack network in barrel U-3000.





(a) Bore surface sample, note reaction zone over entire surface, Unetched, 500X.



(b) Transverse sample, reaction zone lining crack. Unetched, 1000X.

FIGURE 29. Photomicrographs depicting the reaction zone in barrel U-3000.

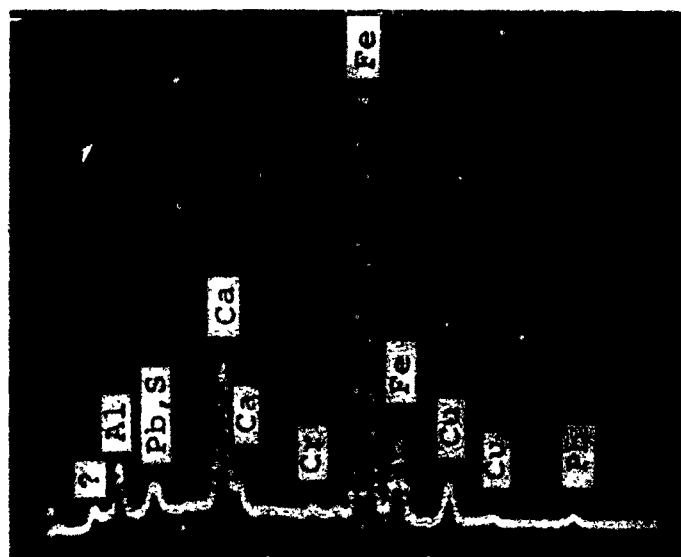
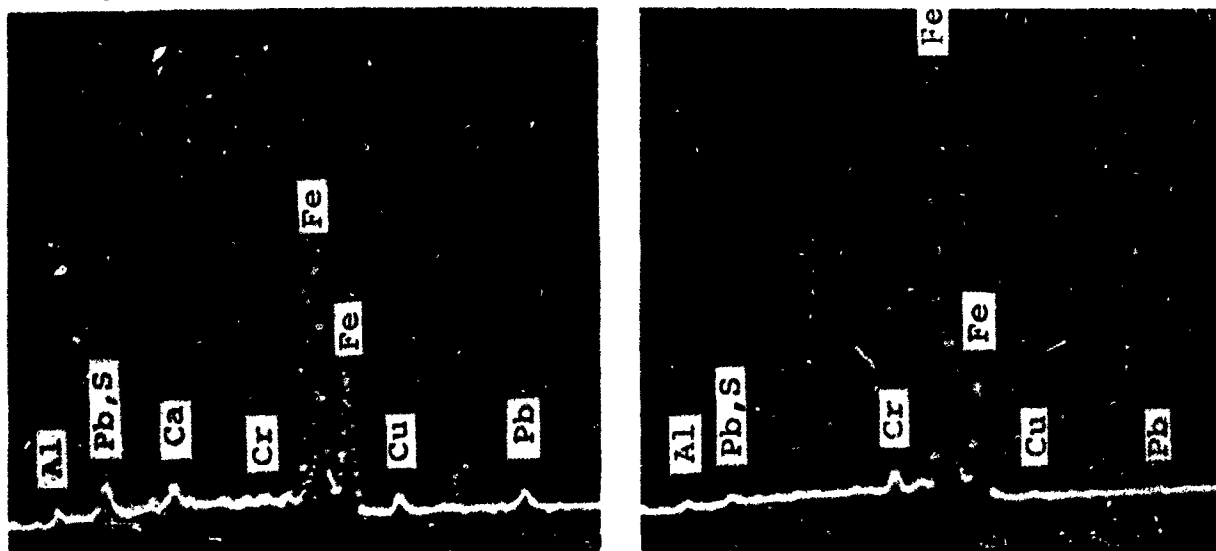


FIGURE 30. Chemical analysis of bore surface of barrel U-3000 (Figure 27).



(a) Scanning electron micrograph, 3000X, indicating positions of chemical analyses.



(b) X-ray spectrometer results - crack (left) and reaction zone (right).

FIGURE 31. Chemical analysis of crack and reaction zone in barrel U-3000.



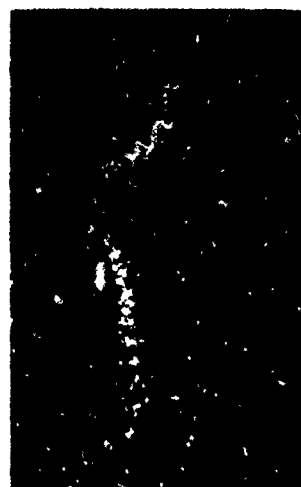
\* Back  
Scattered  
Electrons



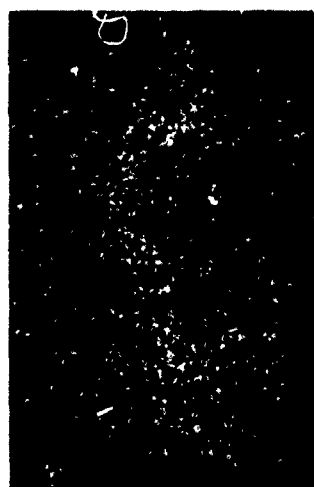
Ca X-rays →



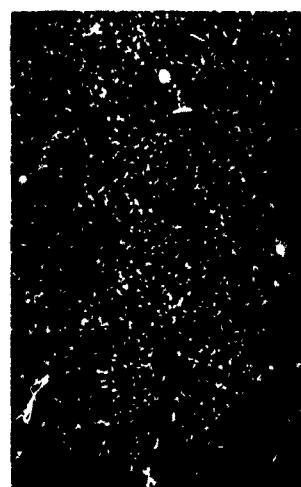
\* S X-rays



Cu X-rays →



\* Pb X-rays



C X-rays →

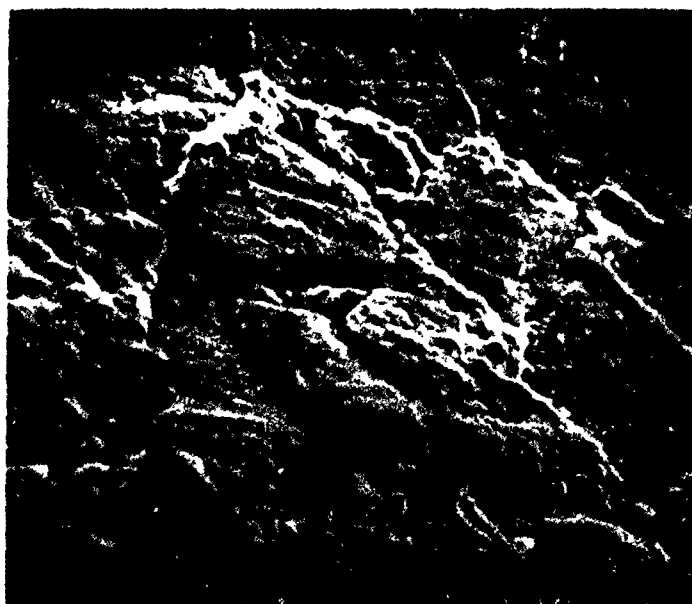
11000x 5.5. Electron microprobe results from  
crack in barrel U-5060. 500x.



FIGURE 33. Crack progression in unplated barrels.  
Transverse samples, 100X. Top U-900,  
Middle U-1500, Bottom U-3000.



(a) Photomicrograph showing Cu throughout cracks in Cr plating. 100X.



(b) Copper assisting in Cr grain removal by wedge effect. Scanning electron micrograph, 300X.

FIGURE 34. Copper deposits in incoherent Cr plating.



(a) Scanning electron micrograph 3000X.



(b) Photomicrograph, 800X.

FIGURE 35. Reaction zone in severely eroded barrels.

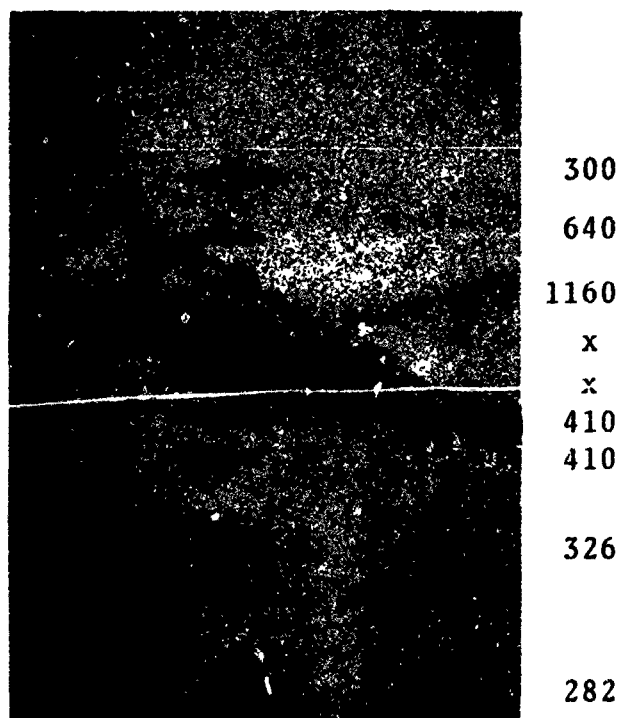
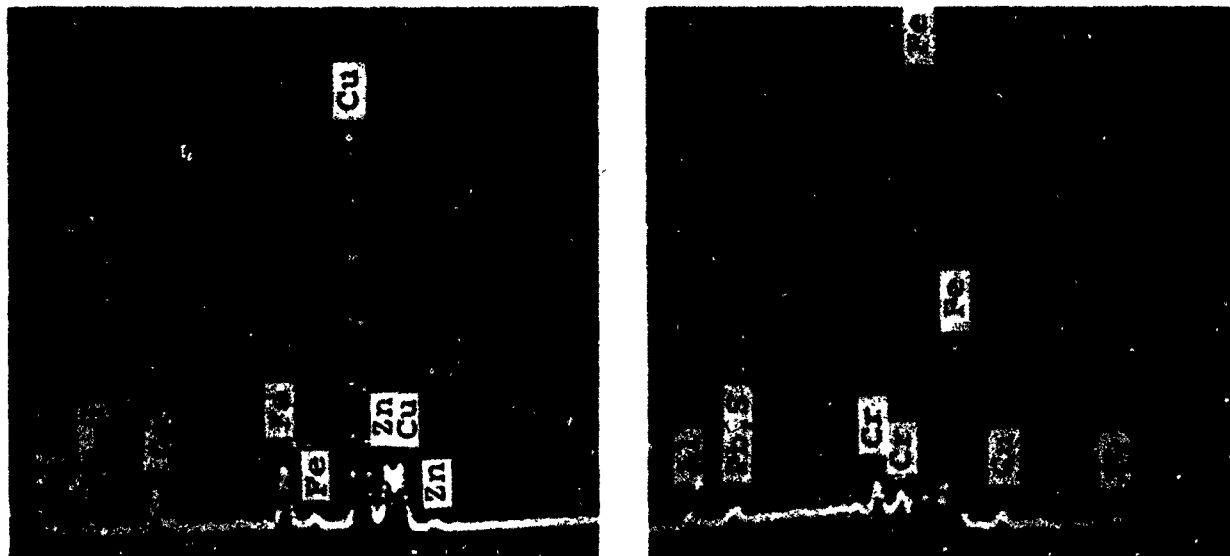


FIGURE 36. Microhardness test (25 gram load).  
Knoop hardness numbers shown. 250X.



(a) Scanning electron micrograph indicating positions of analysis. 300X.

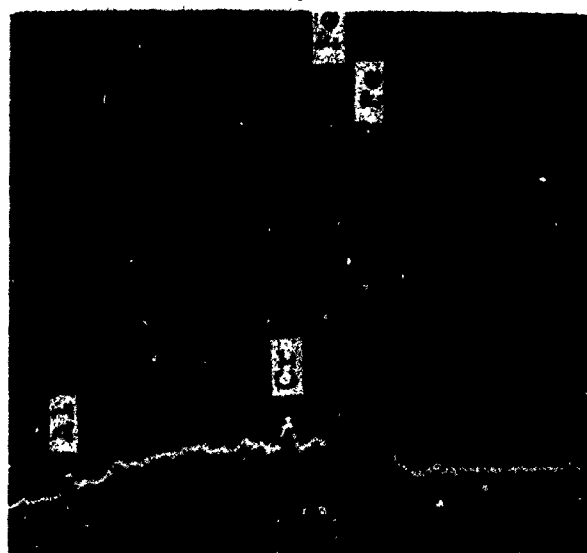
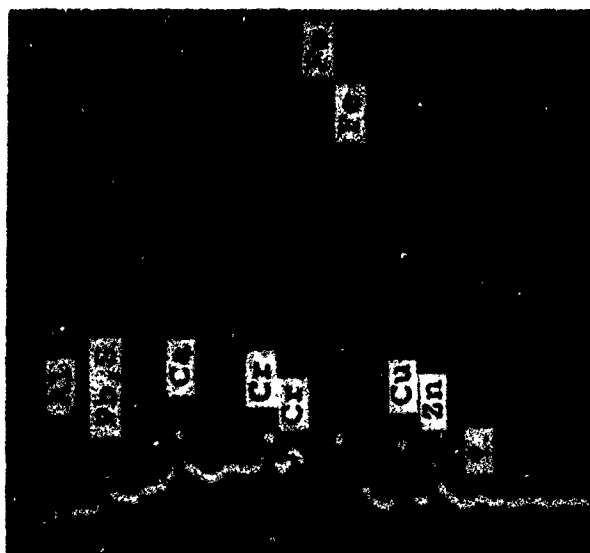


(b) X-ray spectrometer results - crack (left) and representative of reaction zone (right).

FIGURE 37. Chemical analysis of Cu filled crack and reaction zone in severely eroded barrel.



(a) Scanning electron micrograph indicating positions of analysis. 3000X.



(b) X-ray spectrometer results - crack (left) and representative of reaction zone (right).

FIGURE 38. Chemical analysis of crack and reaction zone in severely eroded barrel.





FIGURE 39. Electron microprobe analysis by back scattered electrons of crack network with reaction zone in severely eroded barrel. 500X.

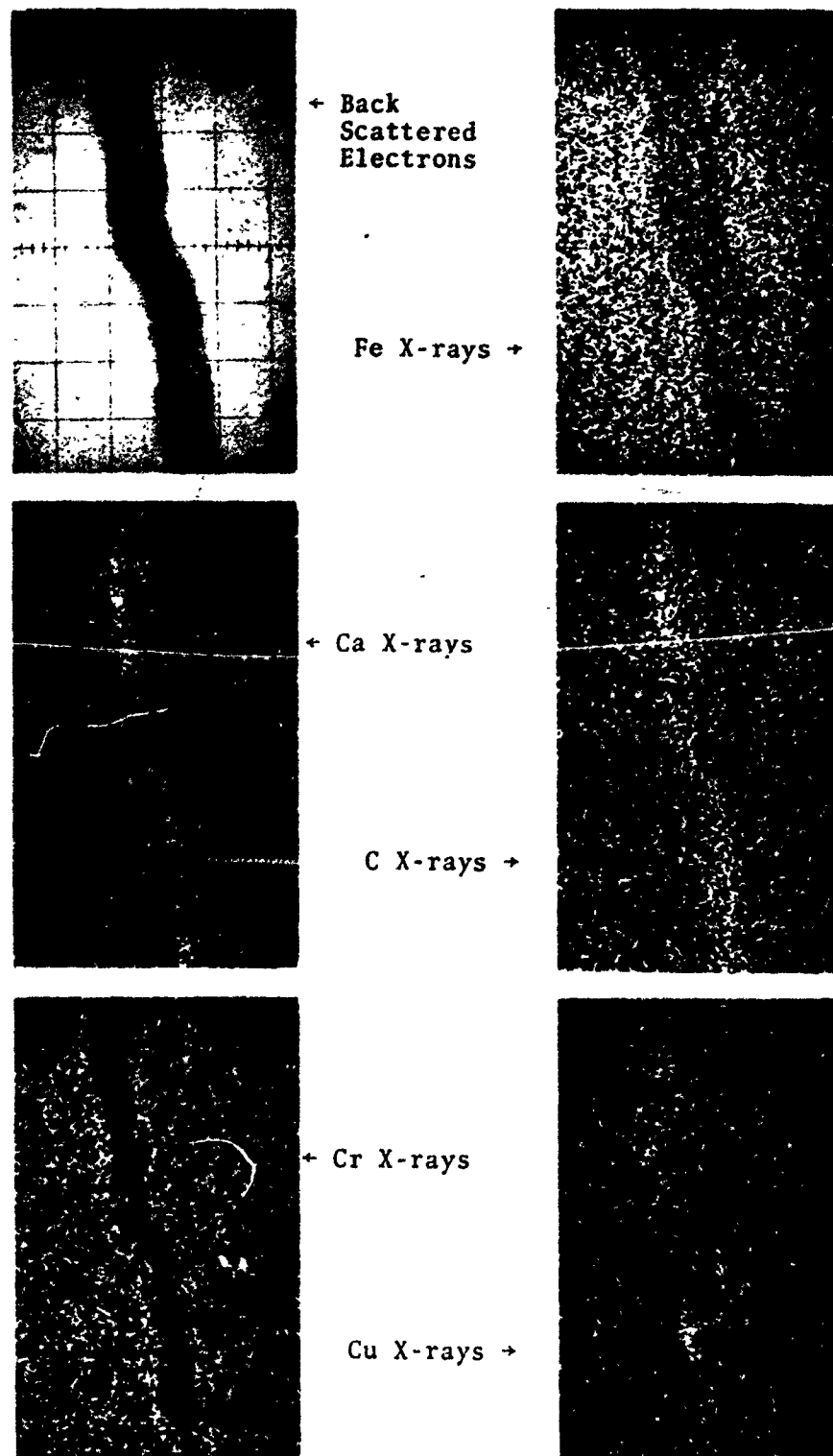
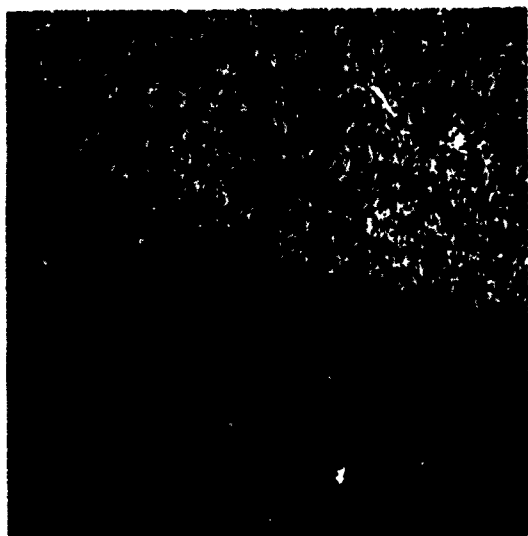
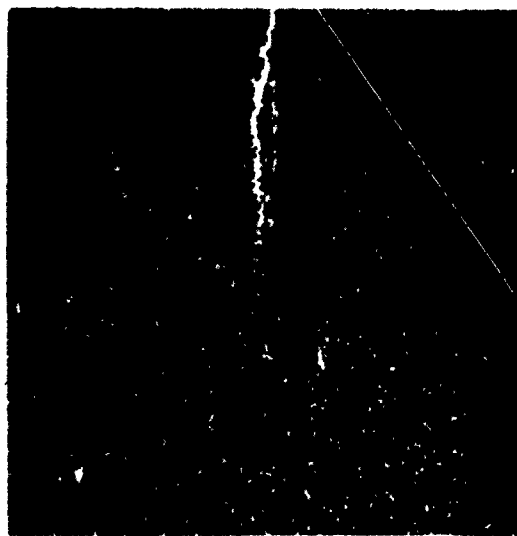


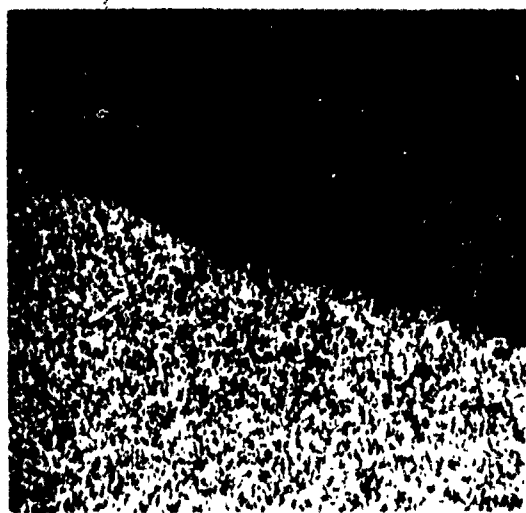
FIGURE 40. Electron microprobe analysis of crack and reaction zone in severely eroded barrel. 1000X.



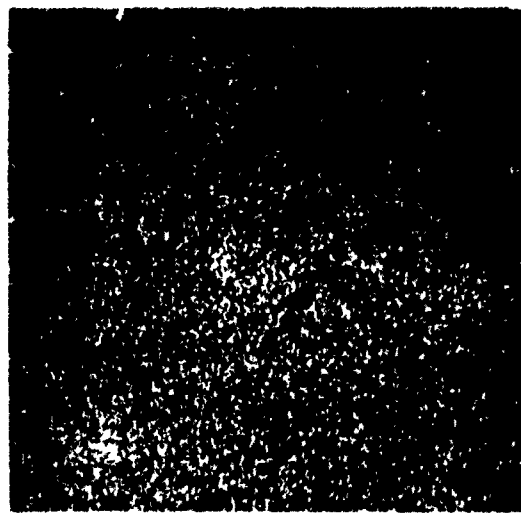
Cr X-rays  
Note crack in Cr plate



Cu X-rays  
Cu filling Cr crack



Fe X-rays  
Note area of reaction zone  
beneath Cr crack



C X-rays  
Increase in C in reaction  
zone at base of crack  
in Cr

FIGURE 41. Electron microprobe analysis of a hemispherical shaped reaction zone in the steel at the base of an existing crack in chromium plate. (1000X)

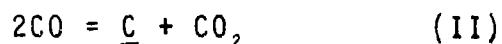
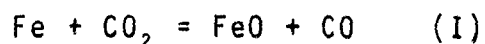
## PART II FATIGUE BEHAVIOR IN REACTIVE ENVIRONMENTS

### A. INTRODUCTION

Cracks observed to develop in small caliber, rapid-fire, machine gun barrels provided the impetus for this investigation. Such cracks limited the performance of these barrels and could have led to catastrophic failure such as that illustrated in Figure 42. The general subject of gun erosion has been reviewed in two major volumes,<sup>3,4</sup> and, although the possible influence of chemical environments on the formation and propagation of cracks has been recognized, it has not been established. In Part I of this report, extensive metallurgical analyses were performed on several test-fired 7.62mm gun barrels. Chemical effects were assumed to be, in large part, responsible for cracking. In addition, micro-cracks, which are inherent in hard chromium electrodeposits,<sup>2</sup> were found to be connected with crack initiation in barrels given this type of plating treatment on the bore surface. This study was undertaken to isolate the effects of CO/CO<sub>2</sub> gas compositions and copper on the cracking of the low alloy, Cr-Mo-V steel at elevated temperature.

The effect of gas composition is of interest because an altered zone, believed to be the result of gas-metal reaction, has been observed around the cracks. Carbon monoxide and carbon dioxide are major components of spent propellant, and a high CO/CO<sub>2</sub> ratio has been reported to be desirable.<sup>3,\*</sup> Numerous factors were considered in the selection of the test temperature of 1000°C. Since a steep temperature gradient exists on the surfaces in contact with propellant gases, note that this temperature (1000°C) is intended to be representative of only a thin surface zone surrounding a crack.

Alloys of iron and carbon will react with the above-listed gases as follows:



With the values given by Gurry,<sup>8</sup> for the equilibrium constants  $K_I$  and  $K_{II}$ , and the activity of carbon in austenite,  $A_{\text{C}_\gamma}$ , the equilibrium gas compositions for the two reactions have been calculated for 1000°C (Figure 43).

Several additional factors must be considered in the oxidation of alloy steels and because of this, analysis of the mechanisms of oxidation is considerably more complex. The general subject of alloy oxidation has been treated in many reviews.<sup>9-11</sup> Also, alloying elements affect the carburizing behavior of steels. Chipman and Brush<sup>12</sup> reported a decrease in the  $A_{\gamma}$  at 1000°C in the presence of the alloying elements of Cr, Mo, V, and Mn which would shift the equilibrium line for reaction II to the right in Figure 43.

The presence of copper observed to be associated with the cracks is of significance because the tendency of liquid copper and copper base alloys to penetrate the grain boundaries of steel is well documented.<sup>13-16</sup>

A search of the literature yielded little information on similar studies on low alloy steels in the vicinity of 1000°C. High-strain fatigue tests on low alloy Cr-Mo-V steels at temperatures up to 700°C have been performed by Coles, et al,<sup>17</sup> Hill,<sup>18</sup> and Krempf and Walker.<sup>19</sup> Environmental conditions, specifically those contributing to oxidation, are postulated as possible factors in the mechanism of failure in each of these investigations. Numerous other studies concerned the effect of gaseous environments on crack initiation and propagation in a variety of alloys under cyclic stress at elevated temperature.<sup>20-25</sup> The results are summarized as follows: Tests performed in a vacuum were generally superior to those in air. In some cases, crack nucleation was associated with pronounced localized oxidation, and subsequent intergranular crack propagation was accomplished by oxidation or attributed to oxygen adsorption.

## B. EXPERIMENTAL PROCEDURE

### a. Apparatus:

A laboratory apparatus was designed and constructed which permitted the high temperature testing of Cr-Mo-V gun steel under alternating stress in selected environments. An overall view of this apparatus is found in Figure 44. The essential elements of this apparatus are shown in the block diagram of Figure 45. The apparatus can be separated into functional categories consisting of: (1) test chamber, (2) induction heating unit, (3) stress application mechanism, (4) temperature control, and (5) environment control. Each of these is described in detail below:

### 1. Test chamber.

The test chamber was a vacuum tight enclosure which contained the hot test specimen (described later) being alternately stressed (tension-compression) as a cantilever beam. A detailed drawing of the chamber with a specimen in place is illustrated in Figure 46. In addition to the forced air cooling of the entire chamber, the top lid had to be water-cooled with a single loop of flattened 1/4" O.D. copper tubing. The joint between the Plexiglas insulation plug and the induction coil leads was sealed with Apiezon putty.

### 2. Induction heating unit.

A high frequency (450 kc) generator equipped with a saturable core reactor for output control coupled to a suitable coil provided for induction heating of the specimen. The generator was a Lepel Model T-5-3-KC-J-B with a maximum rated output of 5 KW. The coil used for heating the specimen was made from 3/10" O.D. copper tubing and contained four turns distributed over a total length of 1-1/4 inches. The coil is shown in Figure 47 with a heated specimen at 1000°C. The representative temperature profiles for the specimen are shown in Figure 48.

### 3. Stress application mechanism.

A unique feature of the apparatus is the utilization of electromagnets to accomplish the desired stress pattern. Power was alternated via a DPDT relay between two diametrically opposite electromagnets thereby attracting the extension rod to first one side and then the other. The electromagnets required cooling by small blowers. The frequency of cycling was adjustable from 100 to 500 cycles per minute, one cycle being a complete tension-compression-tension sequence. An electrical impulse counter registered total cycles and was checked against a timer showing elapsed time.

The extent of travel, i.e., the stress amplitude, was controlled by the stops in the fixture attached to the bottom plate of the test chamber, Figures 46 and 47. The maximum stress can be calculated by:

$$\sigma = \frac{3d \cdot E \cdot r}{l^2}$$

$\sigma$  = stress  
d = distance traveled before hitting stop  
E = modulus of elasticity  
r = radius of specimen (gage section)  
l = distance from gage section to stops

Inserting the values of  $d = 1/16"$ ,  $E = 15 \times 10^6$  at  $1000^\circ\text{C}$ ,  $r = 0.1"$  and  $l = 3.7"$  into this equation yields a value for  $\sigma$  of 21,000 psi. This exceeded the yield strength for this material at  $1000^\circ\text{C}$  so the stress was in the plastic range. No attempt was made to determine the actual plastic strain involved in these experiments.

#### 4. Temperature control.

Temperature measurement was made with an Ircon Model 300T5C infrared radiation pyrometer and temperature indicating unit. An accessory fine focus lens was used which allowed accurate sighting of the pyrometer on a spot as small as .019 inch in the focal range 4-7 inches from the target. The 0-10 MV output from the above instrument was fed into a current adjusting recorder-controller (L & N Series 80). The interface needed between the output of the recorder-controller (0-5ma) and the input to the saturable core reactor (0-80v) of the induction generator was provided by a L & N Series 11900 silicon controlled rectifier power package modified for an inductive load.

The development of a satisfactory temperature measuring procedure and calibration of the radiation pyrometer required considerable effort. Initial attempts to measure temperature directly on the surface of the specimen failed because changing surface conditions made it impossible to accurately determine the emittance value for the surface. Therefore, it was desirable to create a blackbody condition ( $\epsilon = 1$ ) by sighting the radiation pyrometer on a hole drilled in the sample.

The calibration of the radiation pyrometer involved comparison with temperature measured by a Pt-Pt 10% Rh thermocouple. Two holes were drilled in a 1/4" steel rod and a thermocouple was placed in one hole with Pt foil to provide good contact. The pyrometer was focused on the other hole. Agreement of the separately measured temperatures was obtained when an emittance setting of .92 was used which confirmed the hole to be a sufficient blackbody

when the known loss of 8% through the glass walls of the test chamber was considered. Further confidence in this system of temperature measurement was obtained by observation of the melting temperature of silver and copper foils placed in the hole. Silver (M.P. = 1083°C) was observed to melt at 1080°C. All previously described tests were performed with the holes between the second and third turns of the coil. Temperature control during testing was achieved through the use of focusing on a hole in the sample placed between the first and second turns of the coil so as not to interfere with the stress distribution in the gage section of the specimen (Figure 50). This method required the determination of temperature gradients which was accomplished through the heating of a specimen with two holes, one between the first and second turns, the other between the second and third turns, thus temperature equilibration and measuring temperature at both holes are allowed. The results of this test are contained in Figure 49 which is the master graph, used in all testing to determine the relationship between the set point or control temperature and the actual temperature in the gage section. Temperature accuracy was judged to be  $\pm 10^{\circ}\text{C}$  at  $1000^{\circ}\text{C}$ .

#### 5. Environment control.

The atmosphere of the reaction chamber was established through the use of high purity compressed gases of argon (99.996%), carbon monoxide (99.7%) and carbon dioxide (99.9%). The test chamber was evacuated prior to the introduction of the gases then re-evacuated after backfilling with the desired gas mixture. When argon was used, the reaction chamber was filled with the gas and the test was made under static conditions after the gas had been vented during heating. When CO, CO<sub>2</sub>, or mixtures of these gases were used, the flowrate was maintained at 40 cc/min. The flow rate and mixing of the gases were governed by Matheson Model 665 Gas Proportioner which blended the gases by individual flowmeters. All gas mixtures were checked and recorded with a Fisher Gas Partitioner (Model 25V) and a Texas Instruments Servoriter II recorder. Gas samples for analyses were obtained through an integral gas sampling valve. Provisions for analysis of exit gases were also available. All CO/CO<sub>2</sub> mixtures were burned after exiting from the test chamber.

#### b. Specimen Preparation and Test Procedure:

Two types of test specimens. Cr plated and unplated, were incorporated in the high temperature studies both of which are represented in Figures 50 and 51. All Cr-Mo-V steel specimens were machined from forged stock from the

same heat. A chemical analysis yielded the following composition:

<u>C</u>	<u>Mn</u>	<u>Si</u>	<u>Cr</u>	<u>Mo</u>	<u>V</u>
.43	.97	.29	1.29	.65	.21

The nonmetallic inclusion orientation was elongated in the axial direction of the specimens. After machining, the specimens were finished to a 600 grit surface with emery paper. Unplated specimens were finished to a gage section diameter of .200"  $\pm$ .001" while the specimens to be plated were finished to a diameter of .192"  $\pm$ .001" and subsequently received a standard electrolytic hard chromium plating of a thickness of .003" to .004". A hole, .225" deep and .045" diameter was drilled on the taper of each specimen for temperature measuring purposes as described previously. The specimens were thoroughly cleaned with acetone before using.

The procedure for a typical test included closing the test chamber after assembly of the test specimen, evacuating, backfilling with the desired gas, re-evaluating, and allowing the gas to flow for 15 minutes. At this time, the specimen was heated to the test temperature (generally 1000°C) which required less than 60 seconds, and the cyclic loading was initiated. Most tests were carried to failure. In certain tests, copper was placed on the designated specimens. A fine copper wire was melted in situ at 1100°C in argon and 15 seconds were allowed for the Cu to flow over the surface before the test was continued. The liquid copper readily spread over both the steel and Cr plated surfaces.

### C. RESULTS

Tabulation of the cycles to failure as a function of environmental conditions is found in Table V. Numerous other tests were made which were not carried to complete failure. Examples of failed specimens are shown in Figure 52. All test pieces failed in the upper end of the gage section which was located in the hottest part of the specimen. A graphical presentation of the results contained in Table V is given in Figure 53. An increase in the percentage of carbon monoxide retarded failure in both types of specimens, but the effect was more pronounced in the unplated specimens.

# EXPERIMENTAL FATIGUE DATA

<u>Specimen</u>	<u>Environment</u>	<u>Temp. °C</u>	<u>Cycles to Failure</u>
Cr plated	100% CO <sub>2</sub>	1000	9,968
Cr plated	100% CO <sub>2</sub>	1000	8,626
Cr plated	80% CO <sub>2</sub> , 20% CO	1000	10,160
Cr plated	65% CO <sub>2</sub> , 35% CO	1000	15,017
Cr plated	50% CO <sub>2</sub> , 50% CO	1000	12,955
Cr plated	50% CO <sub>2</sub> , 50% CO	1000	17,400
Cr plated	35% CO <sub>2</sub> , 65% CO	1000	14,822
Cr plated	20% CO <sub>2</sub> , 80% CO	1000	15,092
Cr plated	20% CO <sub>2</sub> , 80% CO	1000	23,716
Cr plated	15% CO <sub>2</sub> , 85% CO	1000	26,106
Cr plated	10% CO <sub>2</sub> , 90% CO	1000	27,853
Cr plated	100% CO	1000	19,785
Cr plated	100% CO	1000	28,831
Cr plated	100% CO	1000	31,266
Cr plated	100% CO	1000	26,806
Cr plated	100% Argon	1000	78,068
Cr plated	100% Argon	1000	74,132
Unplated	100% CO <sub>2</sub>	1000	17,791
Unplated	100% CO <sub>2</sub>	1000	19,132
Unplated	80% CO <sub>2</sub> , 20% CO	1000	22,158
Unplated	50% CO <sub>2</sub> , 50% CO	1000	29,608
Unplated	50% CO <sub>2</sub> , 50% CO	1000	35,324
Unplated	20% CO <sub>2</sub> , 80% CO	1000	49,618
Unplated	20% CO <sub>2</sub> , 80% CO	1000	38,572
Unplated	100% CO	1000	74,204
Unplated	100% CO	1000	68,009
Unplated	100% Argon	1000	75,350
Unplated	100% Argon	1100	39
Unplated	100% Argon	1100	38
Cr plated	100% Argon	1100	34
Unplated	100% Argon	1100	10,000

The chromium-plated specimens exhibited inferior specimen life in all ratios of CO and CO<sub>2</sub>; however, in argon the cycles to failure for plated and unplated specimens were comparable.

Metallography and scanning of the electron microscopy on longitudinal sections were used to reveal the structural nature of the cracking. Note that the effects to be described concerning cracks apply in all cases to the fracture surfaces. In high CO<sub>2</sub> (>50%) gas mixtures, both plated and unplated specimens, develop large oxide-filled pits which lead to cracking. This is shown in Figures 54 and 55. As seen in Figure 54, the chromium remains intact with pits developing in the steel through the existing cracks in the Cr plating. The appearance after the etching of a crack representative of those found in the high CO<sub>2</sub> specimens is shown in Figure 56. Ferrite exhibiting a decarburized structure, a dark etching mottled or oxygen-affected zone, and oxide lining the crack surfaces are all in evidence. Oxide, which filled or lined all of the cracks, was very much in evidence at high magnification, Figure 57 in the leading tip of the crack. The mottled zone in the base metal which is apparent in Figure 56 and even more clearly shown in Figure 57 was not observed in 100% CO<sub>2</sub>, but gradually increased when the gas composition was shifted from 80% CO<sub>2</sub> to 50% CO<sub>2</sub>. Decarburization of the steel also increased with decreasing CO<sub>2</sub> which is opposite to what was expected considering reaction I. However, scale formation is known to provide protection against decarburization of the steel substrate.<sup>26</sup>

Some oxide pits were observed at 50% CO<sub>2</sub>. However, below this gas content cracking in the absence of pitting became increasingly prevalent. This condition is illustrated in Figures 58 and 59. Oxide (scale) remained in abundance at 50% CO<sub>2</sub>, but completely disappeared by 20% CO<sub>2</sub>. In this range, and at 10% CO<sub>2</sub>, the mottled zone in the steel became more developed, the particles grew coarser and a preference for formation in the grain boundary was noticed. Such a zone at 20% CO<sub>2</sub> over the surface of an unplated specimen is represented in Figure 60. The mottled zone at the root of a crack is shown in Figure 61. This zone was characteristic of all surfaces exposed to the gas, including the fracture surface. Decarburization continues to increase upon decreasing CO<sub>2</sub> content from 50% to 20% CO<sub>2</sub>. The unplated specimens exhibited few cracks in CO<sub>2</sub> contents of 50% or more. Some failed specimens had no secondary cracks, containing a singular crack which propagated to complete failure. In contrast to the unplated specimens, Cr-plated specimens were always observed to contain numerous cracks.

Tests in 100% CO yielded cracks which in most cases were somewhat finer than those previously described. Again, the mottled zone was apparent on the unetched sample (Figure 62). On etching, (Figure 63), the structure was seen to be altered around the cracks. Microhardness determinations indicated this area to be softer than the martensitic matrix.

The appearance of the mottled zone, shown in Figure 64 and 65 led to an analysis to identify the particles located in this zone. Analysis in which the nondispersive X-ray spectrometer accessory of a scanning electron microscope is used resulted in detection (Figure 66) of the elements Fe, Cr, Mn, and V in the particles. Occasional traces of Mo were also detected. Only Fe and sometimes very small amounts of Cr were found in the matrix or the mottled zone. The relative amounts of the elements Cr, Mn, and V in a particle were observed to increase with decreasing % CO<sub>2</sub>. These results were further verified with the electron microprobe. X-ray scans produced discrete areas corresponding to the particles, which were high in Cr, Mn and V content. In addition, the microprobe results established the mottled zone to be enriched by oxygen, as shown in Figure 67a and 67b. No carbon concentration indicative of carburization was located.

Metallography was extended to the tests made in argon. The cracks, Figure 68, tended to be more blunt. A faint mottled zone was observed on most of the specimens, but diminished on the fracture surfaces. A two-layer diffusion zone formed between the steel and the Cr in all plated specimens. Cracking and separation were common along this zone which in some instances facilitated removal of the plating (Figure 68). These diffusion zones are shown in Figure 69 as they appeared after testing in argon. Identical zones have been identified as the complex carbides (Cr,Fe)<sub>23</sub>C<sub>6</sub> and (Cr,Fe)<sub>7</sub>C<sub>3</sub>.<sup>27</sup>

The topography of the fracture surfaces were studied with the SEM. High CO<sub>2</sub> contents resulted in gross scaling masking of any detail. In the absence of scale formation, all fractures appeared similar, Figure 70 being representative.

Tests made in the presence of liquid copper (above 1100°C) required only 40 cycles before failure occurred. A thin film of copper covered the fracture surface. The extent of intergranular penetration of copper to which failure can be attributed is clearly shown in Figures 71 and 72. No difference between the Cr plated and unplated samples was observed. Although no tests were continued to failure, both plated and unplated samples showed no damage after 10,000 cycles in argon at 1100°C. Also, no detrimental effects were ascribed to

the copper after 10,000 cycles in tests run in argon and  $\text{CO}_2$  at  $1000^\circ\text{C}$ , below the melting point for Cu of  $1083^\circ\text{C}$ .

#### D. DISCUSSION OF RESULTS

The observed effect of the  $\text{CO}/\text{CO}_2$  ratio on the fatigue test results can be entirely attributed to a decreasing oxygen potential in the gas phase with decreasing %  $\text{CO}_2$  (increasing %  $\text{CO}$ ). This, of course, implies that reaction II is insignificant in these results. The rationale that the structural appearance of the zone (Figure 63), characteristic of the 100%  $\text{CO}$  tests, might be due to a carbon pickup, is recognized. Rather, this zone is believed to be simply the result of the transformation of austenite to a higher product (i.e. ferrite + pearlite) which would be appropriate for a matrix zone depleted in the alloying elements which are known to be segregated in discrete particles. After reviewing the decarburization trends, the conclusion is that this zone had minimal relevance to the results.

Assessment of an oxygen potential to a 100%  $\text{CO}$  gas composition requires certain clarification. The gas consisted of  $\text{CO}$  upon entering the chamber, but the instability of the gas resulted in deposition of carbon (soot) and generation of some  $\text{CO}_2$ . Carbon deposition at higher  $\text{CO}$  contents was common and traces of  $\text{CO}_2$  were present in the exit gases of the 100%  $\text{CO}$  tests.

Oxide formation was observed on all specimens with greater than the equilibrium value of  $\text{CO}_2$ , as expected from reaction I. These oxides were not magnetic, consequently wüstite was assumed to be the predominant oxide form. A straight line fits the data (Figure 53) in the range of iron oxidation (30%  $\text{CO}_2$ ). The kinetics and mechanisms of the oxidation of iron in carbon monoxide-carbon dioxide atmospheres has been investigated by Smeltzer,<sup>28,29</sup> Pettit, et al.<sup>30,31</sup> The initial oxidation rate was determined to be linearly proportional to the partial pressure of  $\text{CO}_2$  above the equilibrium value. In this linear region, the rate determining step is represented by dissociation of  $\text{CO}_2$  on the surface into chemisorbed oxygen and  $\text{CO}$  gas. Attempts at a more rigorous correlation between the rate of oxidation and the present results were unsuccessful because of insufficient data. However, the mechanism of fracturing in the region of external oxidation is not a simple sequence of oxide formation, cracking of the brittle oxide exposing fresh surfaces, reformation

of the oxide, etc. This mechanistic approach was eliminated on the basis of calculations which established scale formation to be too slow to satisfy such an approach. The explanation of Achter and co-workers<sup>22,24,25</sup> relies on surface absorption of gaseous impurities resulting in a reduction of surface energy which facilitates crack propagation. After detailed studies of superalloys, Coffin<sup>20,21,23</sup> proposed that strain-induced oxidation is the cause of crack nucleation in the form of wedge-shaped oxide intrusions. Crack propagation then takes place intergranularly because oxidation processes proceed more rapidly along these boundaries especially when under the influence of stress. Although the exact nature by which oxidation increases cracking has not been established in the present investigation, the observed results would be in basic agreement with the mechanism attributed above to Coffin.

Heretofore, only external oxidation has been discussed. The analysis indicates that the particles in the mottled zone are complex oxides of Fe, Cr, Mn, and V which are formed by internal oxidation of the steel either with or without external formation of FeO. A schematic representation of the internal oxidation of iron alloys with small alloying additions is shown in Figure 73. Oxygen dissolved in the alloy will selectively oxidize the less noble component forming the internal precipitate which is probably complex Fe-X oxides. Such oxides are thermodynamically favored.<sup>32</sup> Internal oxidation identical to that observed here has previously been reported to occur in similar low alloy steels subjected at high temperature to CO/CO<sub>2</sub> atmospheres.<sup>33,34</sup> The oxide precipitate is also found in the matrix but prefers grain boundary formation. Meijering,<sup>35</sup> on the other hand, rejects preferential penetration along grain boundaries during oxidation of iron. However, dynamic stress conditions of the present tests compared with his static tests can easily account for this discrepancy.

Convincing evidence was presented which leads to the conclusion that cracking follows the grain boundary oxide precipitate (Figures 64 and 65). The effect on the cracking of the internal oxide precipitate when distributed in the matrix is believed to be of secondary importance. Matrix precipitates may possibly provide a form of oxidation strengthening, and retard crack initiation at the surface.

Examination of the role of chromium plating in promoting cracking was centered around the inherent defects in the plating. The initiation stage was intrinsic in the Cr plated

specimens. In argon, however, the results indicate the failure for the plated and unplated conditions are comparable. This assumption is that the propagation stage is comparable in both types of specimens. These results are compatible with those of Manson<sup>36</sup> who predicted intergranular failures at these temperatures with the initiation stage being a minor portion of the total life. Hence, the failure is propagation controlled.

On contemplation of the foregoing, the premise that the effect of the plating in reducing the cycles to failure in an aggressive atmosphere is principally mechanical and is invalid. Undoubtedly, cracks in the Cr assist in initiating cracks in the steel, but the combination of the existing crack and a chemical effect are responsible for premature failure. The chemical contribution was, in these series of tests, the oxidation previously discussed. Correlation of the diffusion zone formation with cracking appeared appropriate considering Figure 63, but the argon results seemed to negate any significance attached to the diffusion zone in affecting the results of these experiments. In the unplated specimens, the cycles to failure increased rapidly at CO<sub>2</sub> contents less than that needed to maintain external oxidation. In fact, with very small amounts of CO<sub>2</sub>, any effect of oxidation diminished and the cycles to failure approached that of the inert atmosphere. In the Cr-plated specimens, however, a definite effect of oxidation persists with even small quantities of CO<sub>2</sub>. These observations show that, in reactive environments, the crack propagation interval decreases to an extent where the crack initiation stage becomes quite significant. Therefore, in Cr-plated specimens where the initiation stage is negligible, the total cycles to failure will be less than that for the unplated specimens where the initiation stage is not negligible.

Liquid Cu grossly reduces the life of this steel due to a form of liquid metal embrittlement. According to Smith,<sup>37</sup> the formation of liquid films at the grain boundaries can be assessed by involving interfacial energy relationships which determine the dihedral angle  $\theta$ , Figure 74. With application of interfacial energy values at 1105°C reported by Van Vlack<sup>38</sup> for liquid copper/austenite of 430 ergs/cm<sup>2</sup> and austenite/austenite of 850 ergs/cm<sup>2</sup>, the relationship provides a dihedral angle approaching 0°. On consideration of the above, the dramatic reduction of cycles to failure in the presence of a small amount of liquid copper observed in this study is to be expected. The tensile portion of each stress cycle greatly improves penetration because it opens the properly oriented boundary offering a more favorable condition for further penetration.

Initially, the conditions of these fatigue tests do not exactly simulate the conditions existing in the gun barrel. A major difference is the kinetic factor with the rates "experienced" in gun barrels being orders of magnitude greater. The assumption, however, is that the trends observed in these laboratory experiments can be qualitatively extrapolated to provide a better understanding of possible chemical changes in the gun barrel.

The conclusion of the work is that, if the copper deposits are liquid at any time, the resultant attack will be catastrophic. Embrittlement by solid copper deposits does not appear to be a primary factor for early "retirement" of rapid-fire 7.62mm steel gun tubes with standard ball ammunition.

The effect of the cracks in the Cr plating in improving preferential chemical attack is probably more pronounced in these experiments than in the actual barrel. The same type of mechanism of concentrated chemical attack at the root of the existing crack would be operative in the Cr-plated barrels. So the conclusion is identical, i.e., radial cracking will be more severe in Cr-plated barrels than in unplated gun tubes. This does not imply that a plated barrel is inferior to the unplated barrel because the uniform wear of the unplated barrels leading to inferior service life has not been accounted for. From these results, logical approach to minimize barrel deterioration would be, apparently, to develop fracture-tough platings. A less obvious, but perhaps more easily attainable solution would be to incorporate a chemically resistant intermediate layer between the plating and substrate which would retard the crack initiation or growth or provide a more chemically resistant gun tube than Cr-Mo-V steel.

The oxygen potential of the gaseous environment was shown to affect the cracking tendency. Certainly, a low oxygen potential is desirable for minimizing deterioration of the barrel. Undetermined factors such as pressure, temperature, and gas composition which exist in the barrel make exact correlations to laboratory results impossible.

It is felt that the most important outcome of these experiments is the qualitative demonstration of how chemical reactivity affects gun barrel material behavior. These findings suggest that additional criteria for evaluation and selection of candidate materials for gun barrels are needed. In addition to the normal thermal and mechanical property considerations, chemical resistance must also be evaluated.



FIGURE 42. Catastrophic failure in 7.62mm gun barrel.

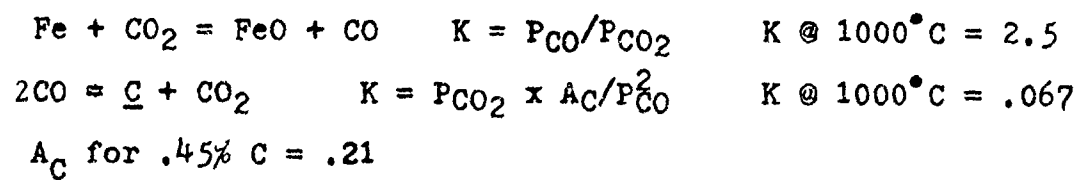
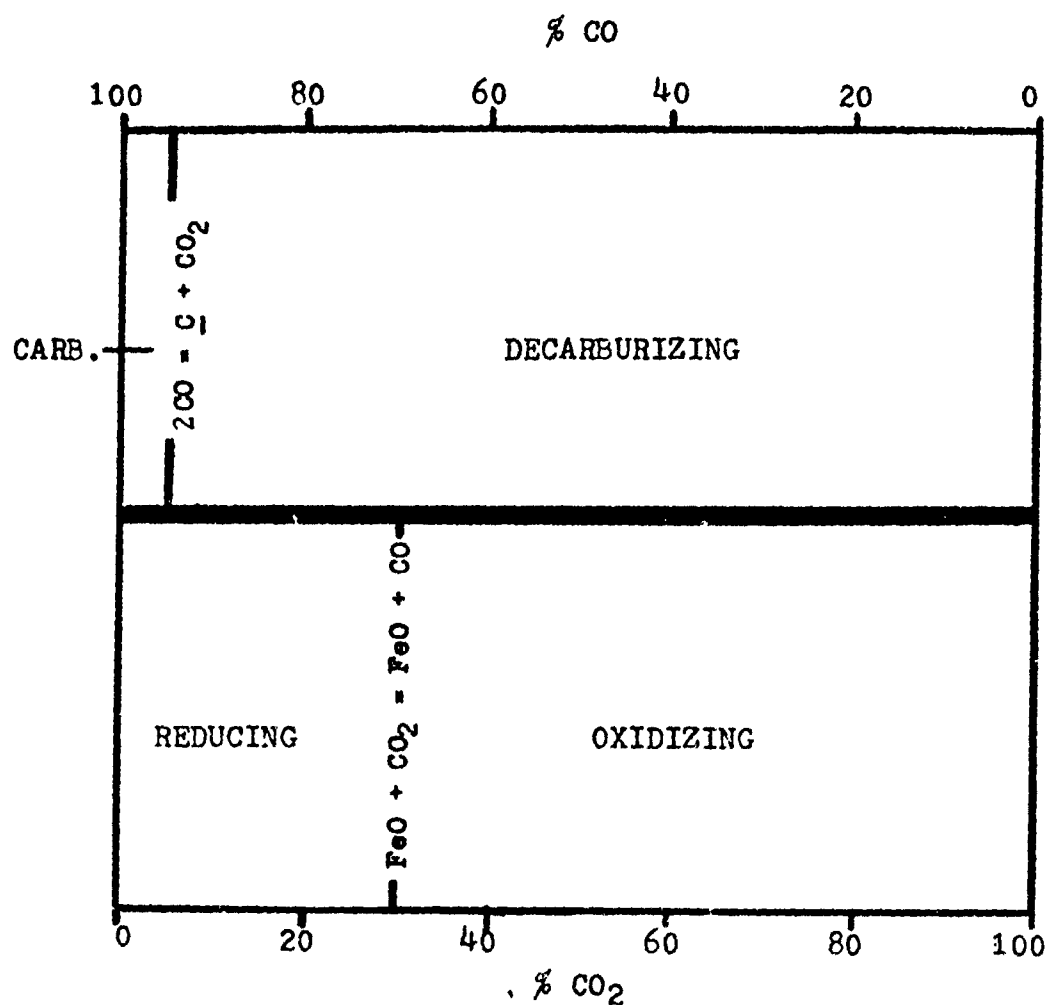


FIGURE 43. Reactions of iron with CO/CO<sub>2</sub> atmospheres.<sup>8</sup>

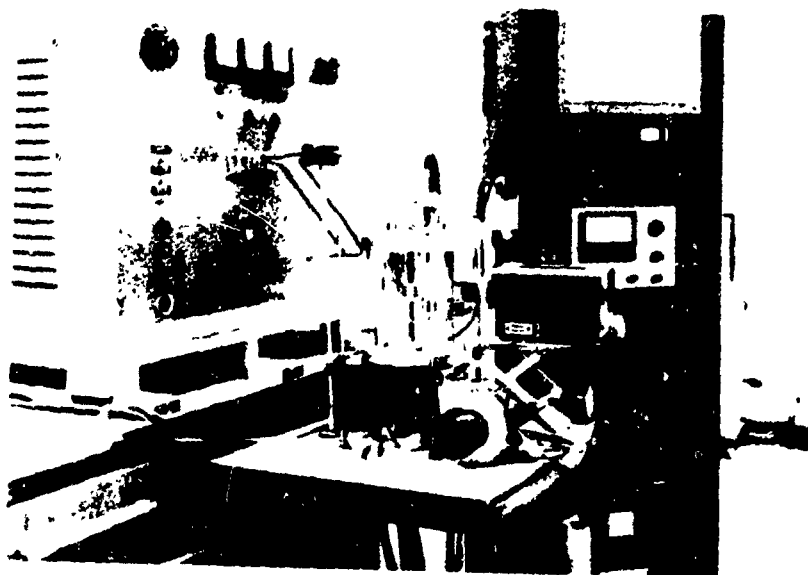


FIGURE 44.      Photograph of apparatus

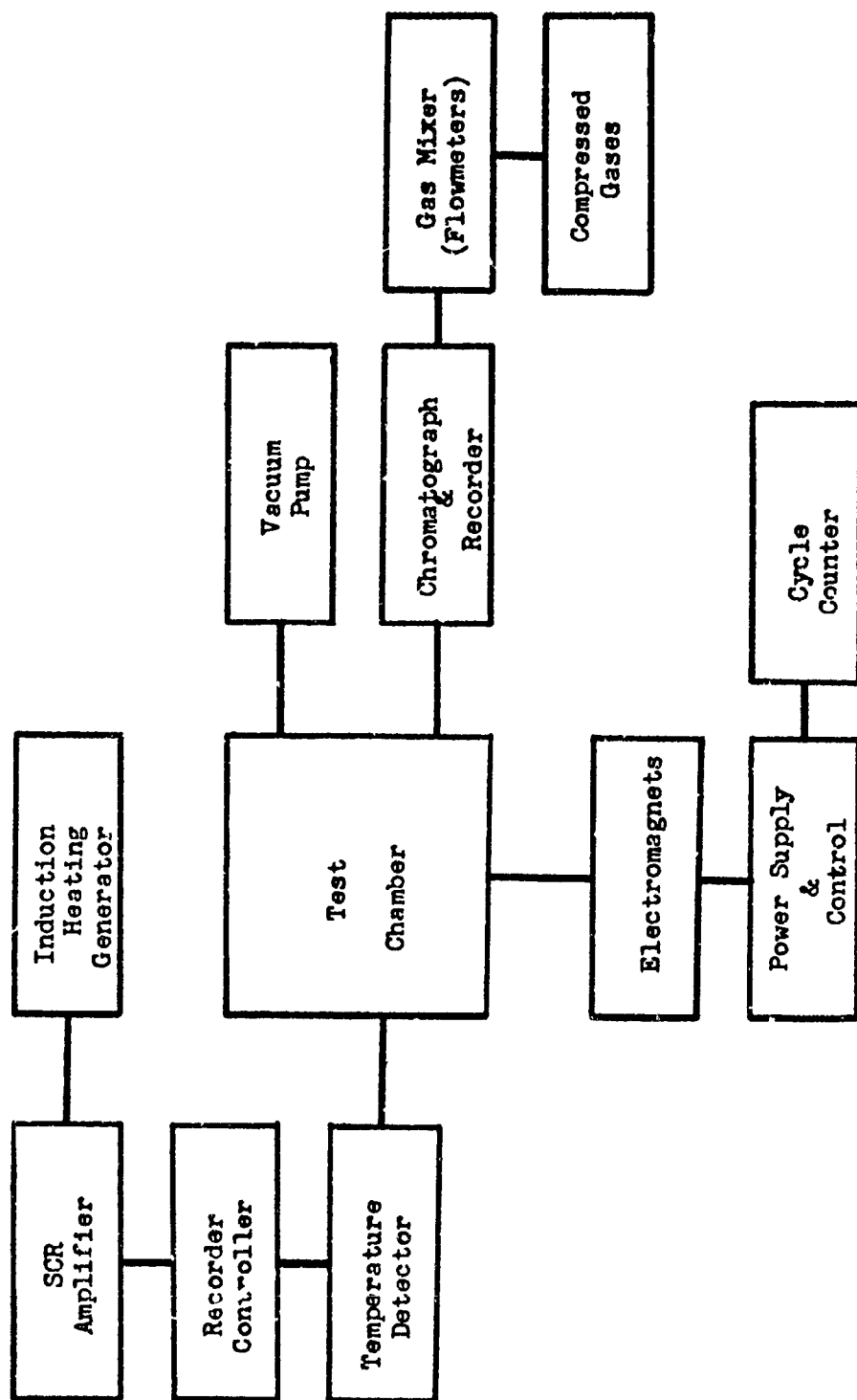


FIGURE 45. Diagram of Apparatus Components.

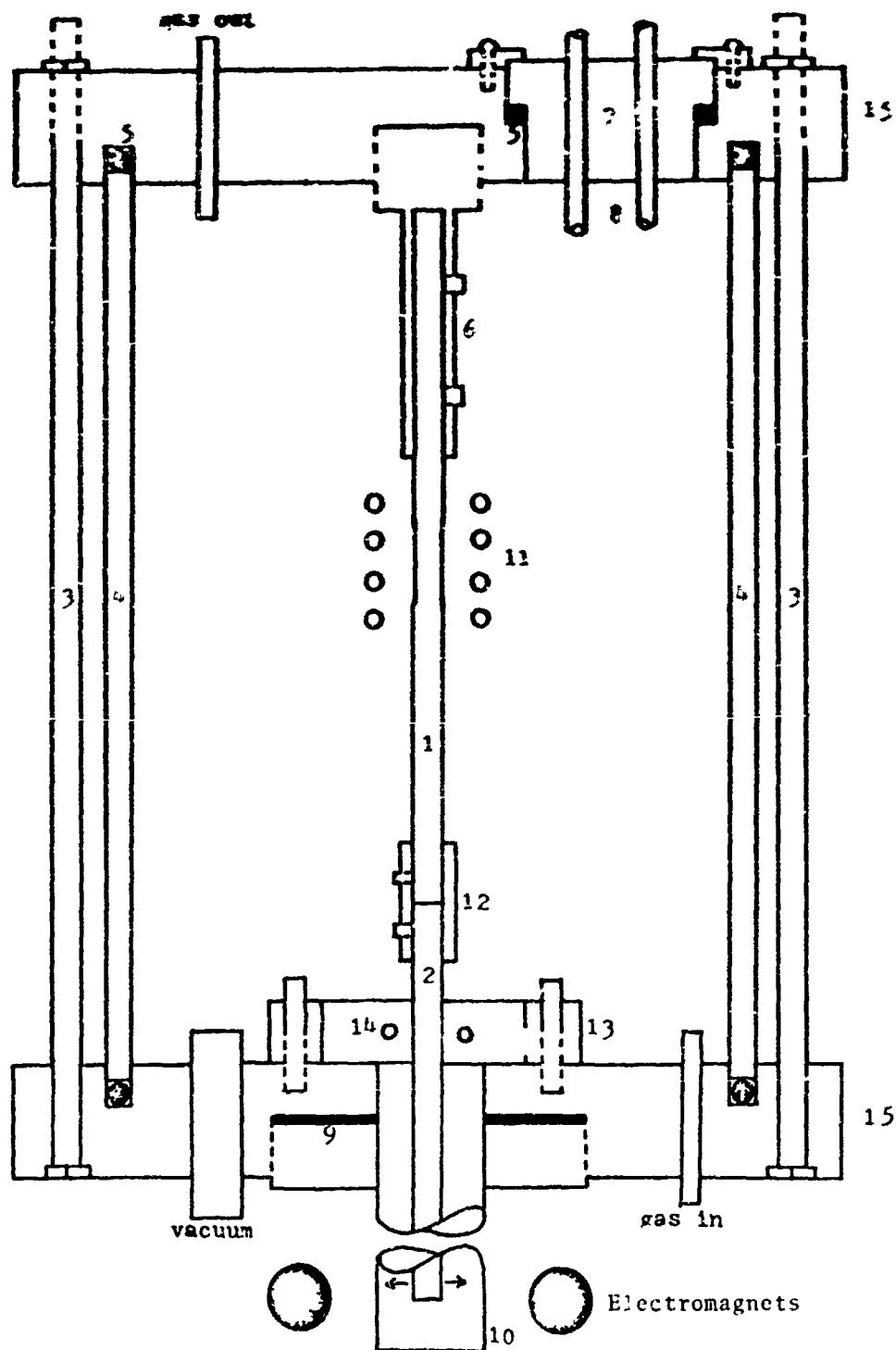


FIGURE 46. Test chamber. 1. specimen 2. specimen extension rod 3. tie rods 4. glass 5. O rings 6. support stud 7. Plexiglas plug 8. induction coil leads 9. gasket 10. hang down tube 11. induction coil 12. coupler 13. specimen guide 14. stress stops 15. Al base & cap



FIGURE 47. Induction coil with specimen at 1000°C.

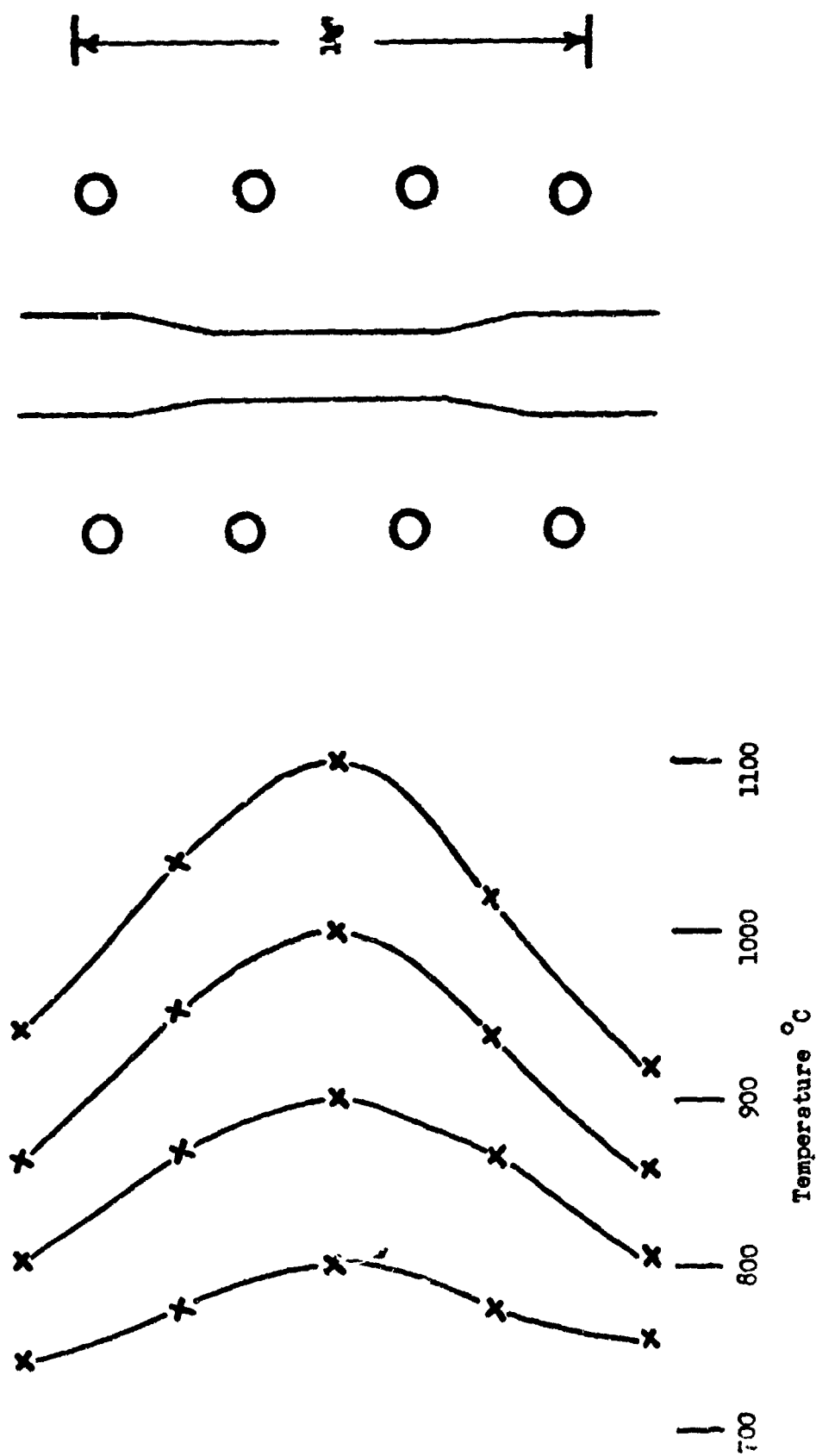


FIGURE 48. Temperature profiles in specimen heated in induction coil.

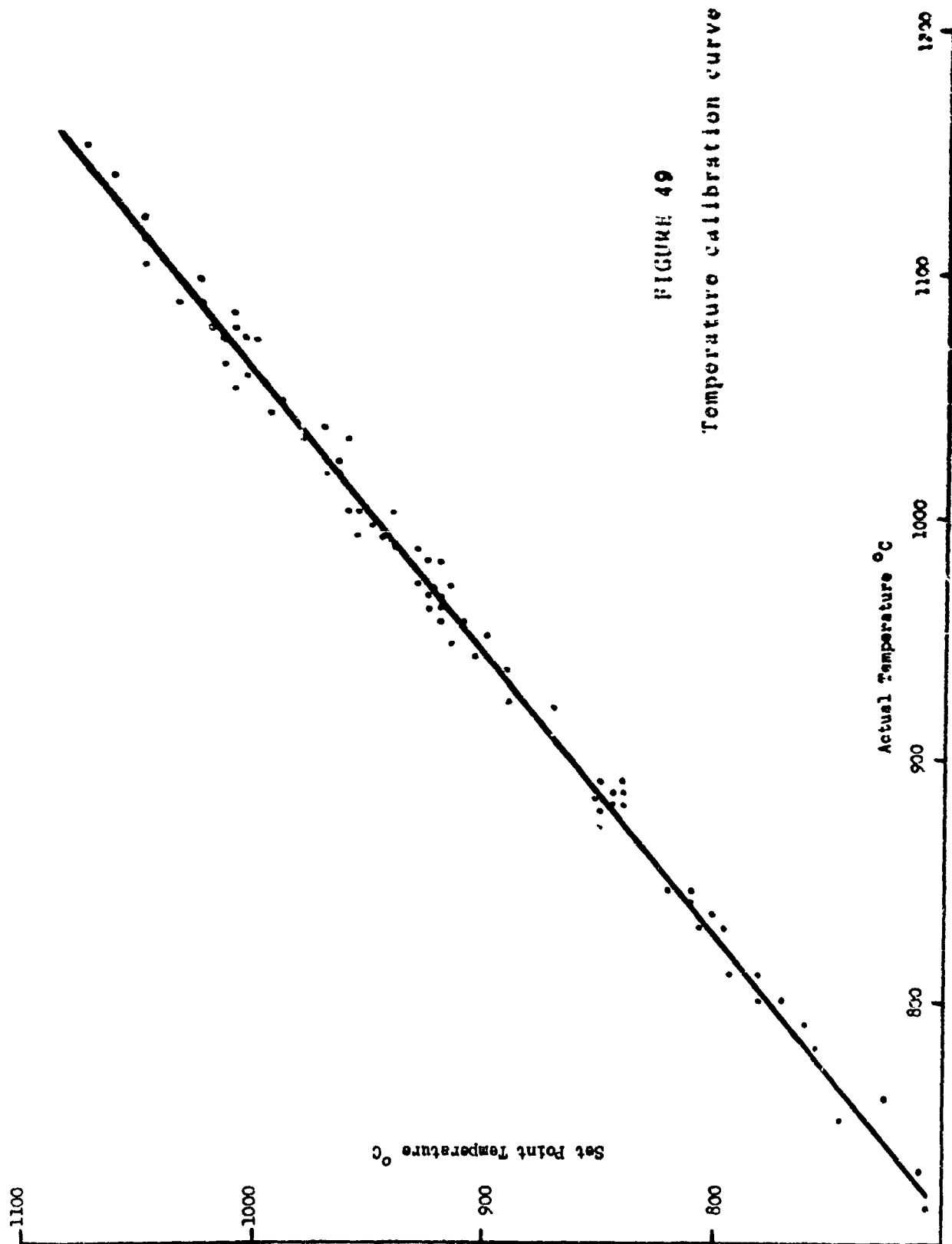


FIGURE 49  
Temperature calibration curve

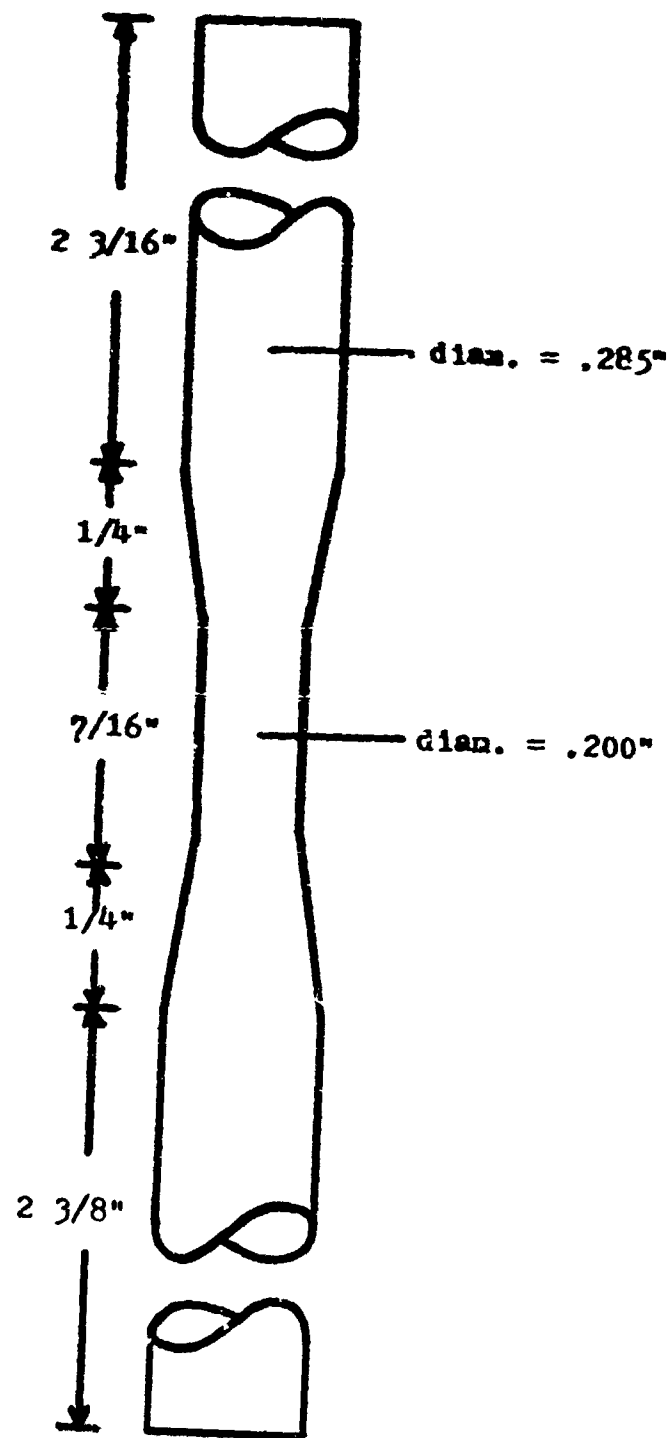


FIGURE 50. Test specimen dimensions.



FIGURE 51. Gage section of test specimens, right unplated; left-Cr plated.

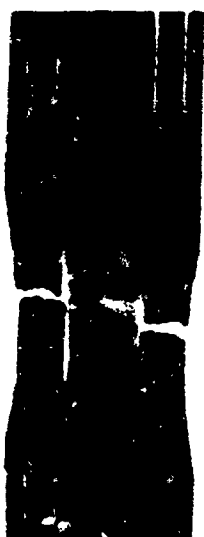


FIGURE 52. Test specimens after failure, right-unplated; left-Cr plated.

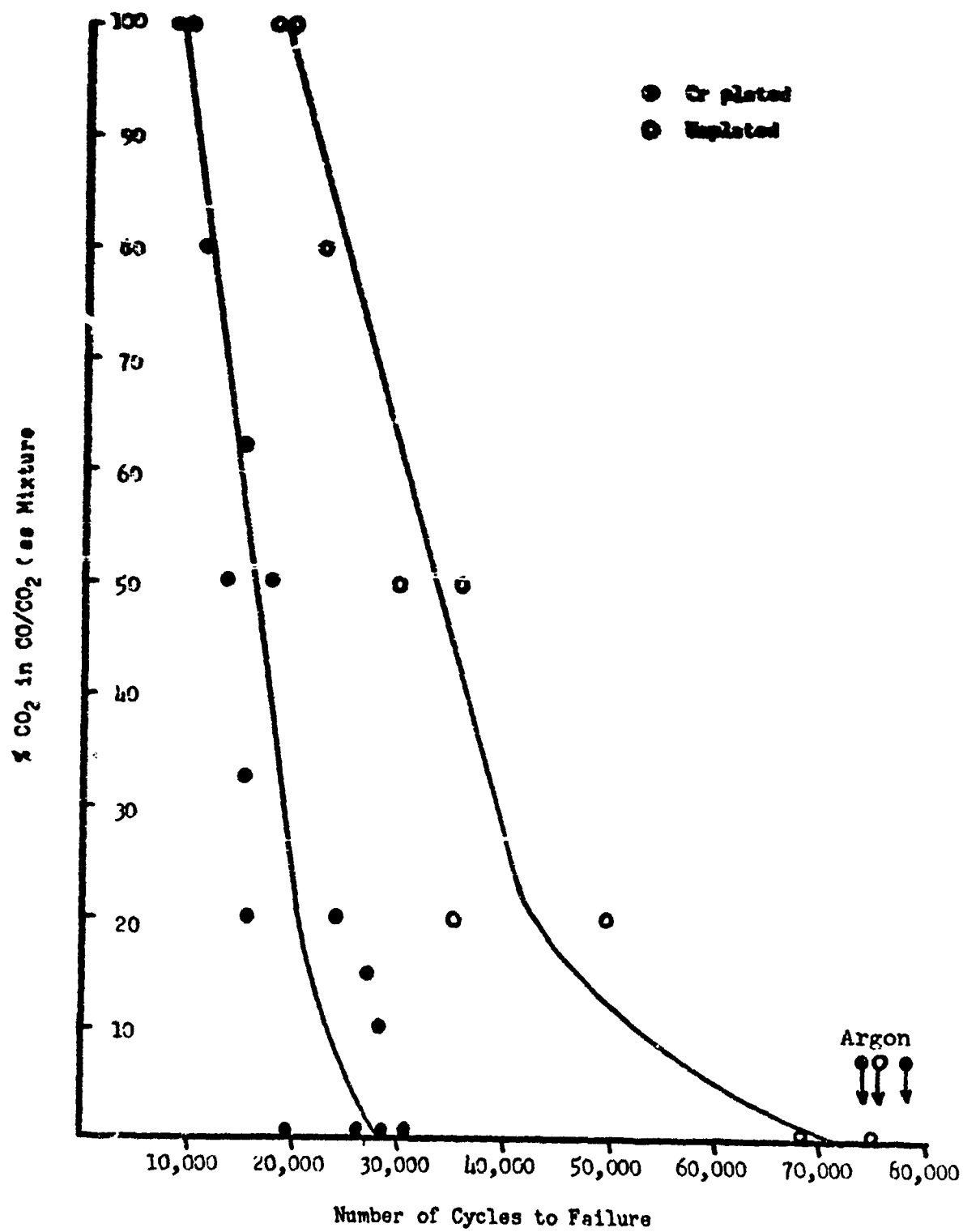


FIGURE 53. Plot of fatigue life as a function of gas composition.



FIGURE 54. Pitting beneath Cr plating typical of high  $\text{CO}_2$  mixtures. 200X.



Figure 55.

Oxide filled crack  
generating from a pit  
in unplated sample.  
100X.



FIGURE 56.

Photomicrograph of  
crack representative  
of high  $\text{CO}_2$  specimens.  
Nital etch. 500X.



FIGURE 57.

Scanning electron  
micrograph of oxide  
in crack and mottled  
zone. 30%  $\text{CO}_2$ . 3000X





FIGURE 58. Crack propagation in the absence of pitting in Cr plated specimen. 500X. 50% CO<sub>2</sub>.



FIGURE 59

Same as above. 200X.



FIGURE 60. Mottled zone on surface of 20% CO<sub>2</sub> specimen,



FIGURE 61.

Intergranular formation  
of precipitate in mottled  
zone formed at crack tip.  
750X.



FIGURE 62. Fine crack in 100% CO specimen. 500X.



FIGURE 63. Altered zone around crack in 100% CO specimen.  
Nital etch. 500X.



FIGURE 64. Scanning electron micrograph of mottled zone. Note crack following intergranular particles. 3000X.



FIGURE 65. Scanning electron micrograph of mottled zone. Note cracking in the particles. 3000X.

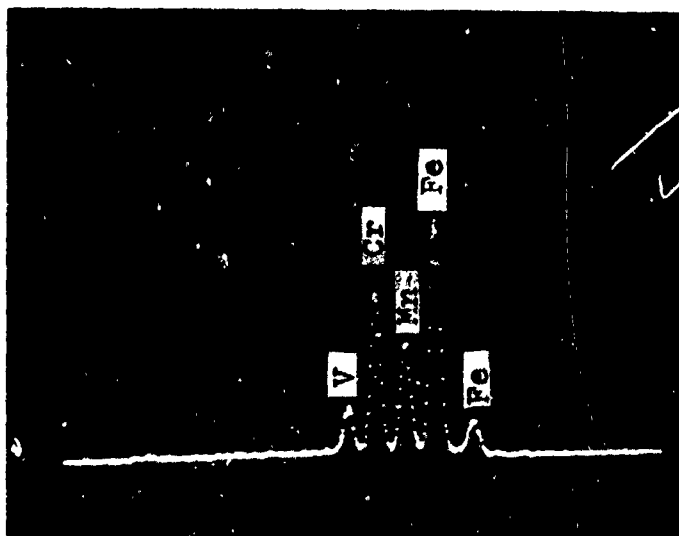
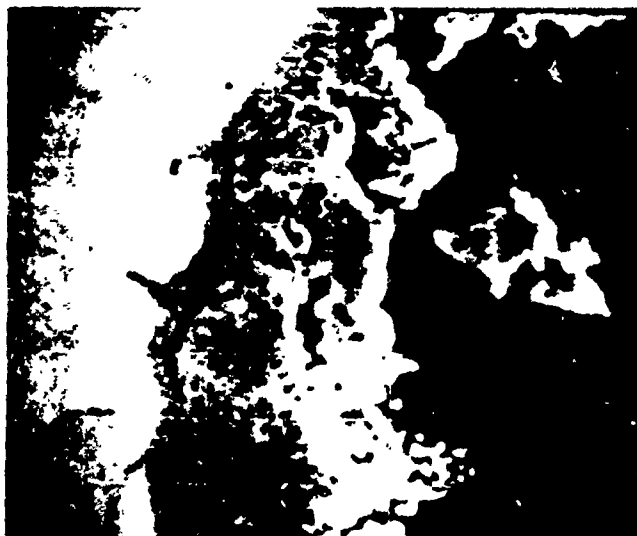
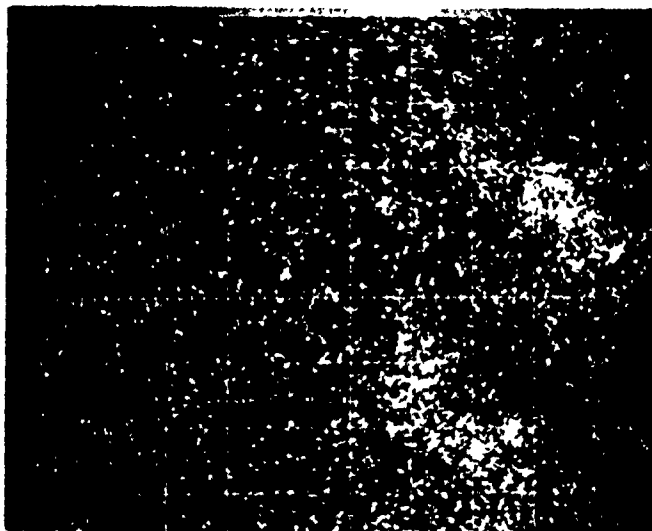


FIGURE 66. X-ray spectrometer analysis of precipitate particles in mottled zone.



a



b

FIGURE 67. Electron microprobe results of the mottled zone. A. Electron image showing the zone to be of lower atomic number. B. Oxygen X-ray image indicating oxygen enrichment. 375X.



FIGURE 68. Blunt cracks in Cr plated specimen tested in argon. 200X.



FIGURE 69. Diffusion zones formed in the Cr plated samples. Note two intermediate zones between Cr (top) and steel (bottom). Nital etch. 500X.

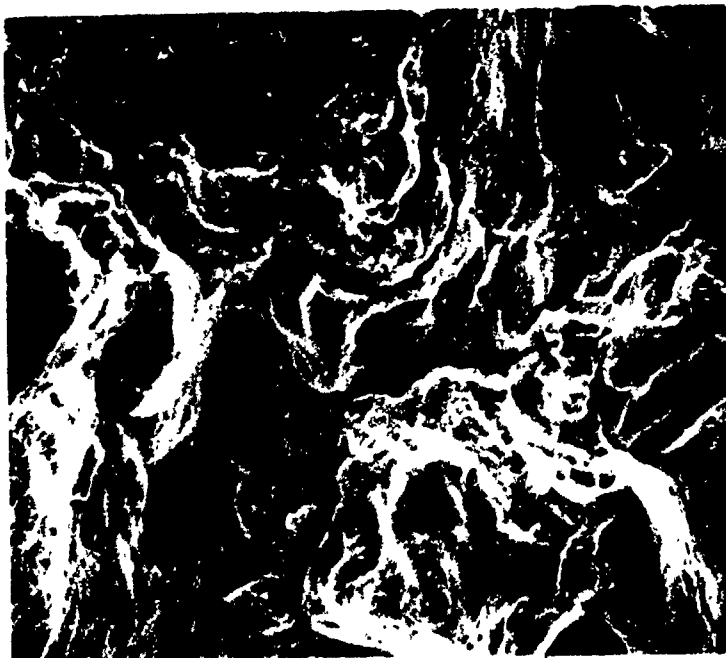


FIGURE 70. Scanning electron micrograph of fracture surface topology. 20% CO<sub>2</sub>. 300X.

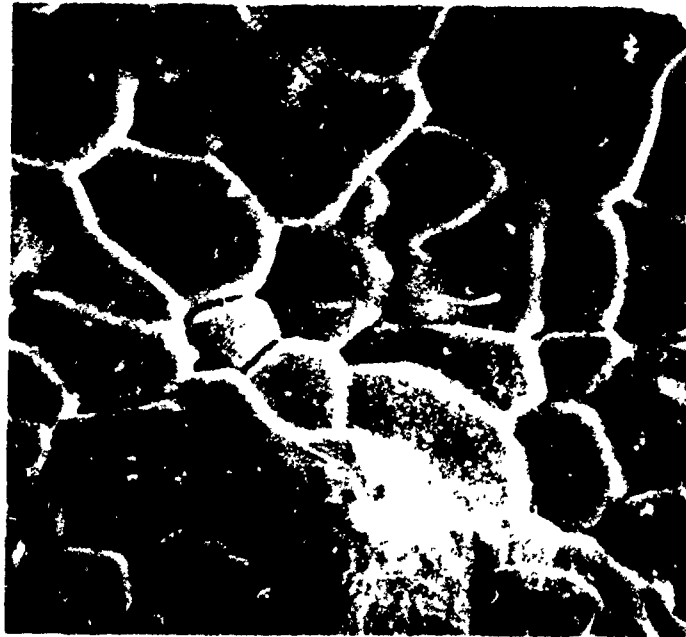


FIGURE 71. Scanning electron micrograph of copper film over fracture surface. Note copper penetration decorating grain boundaries. 600X.

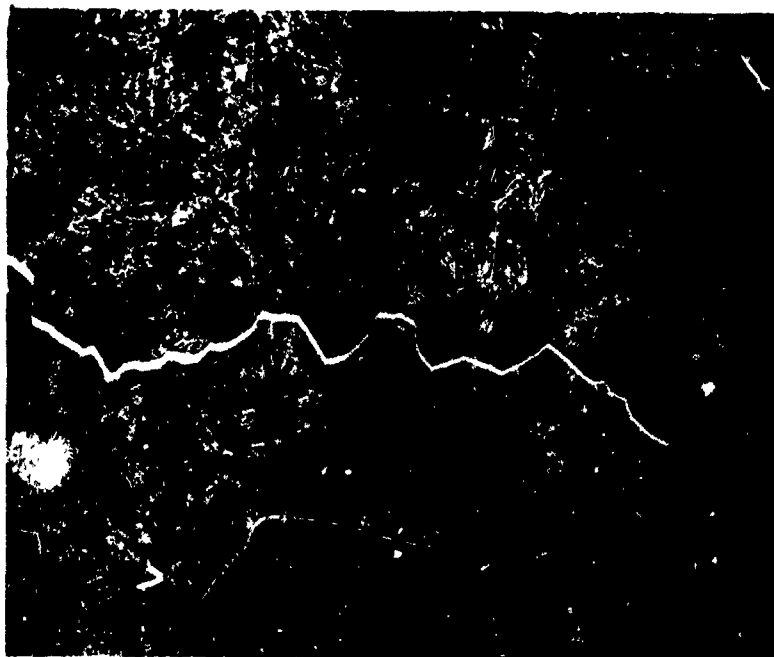


FIGURE 72. Photomicrograph showing liquid Cu penetration which led to rapid failure. Penetration perpendicular to surface of specimen. 150X.

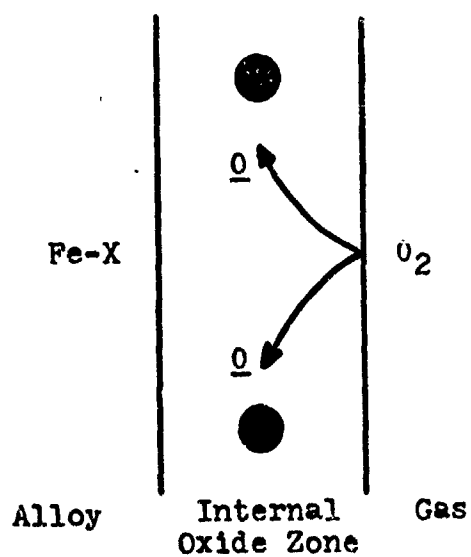
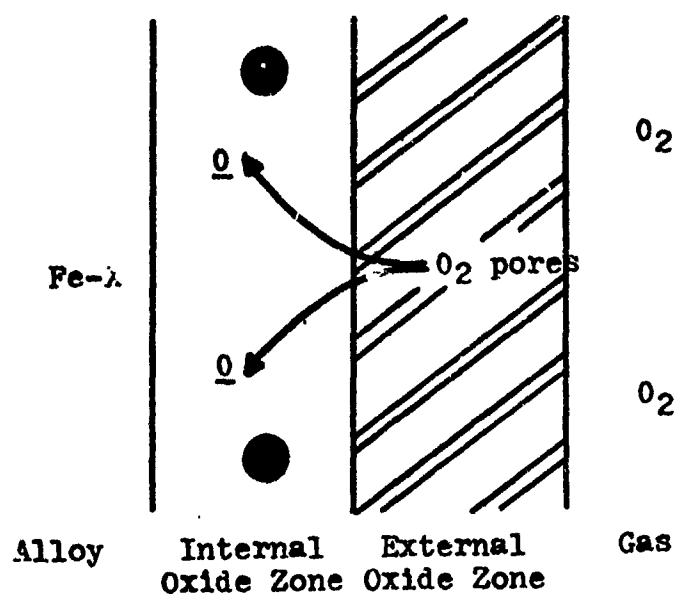
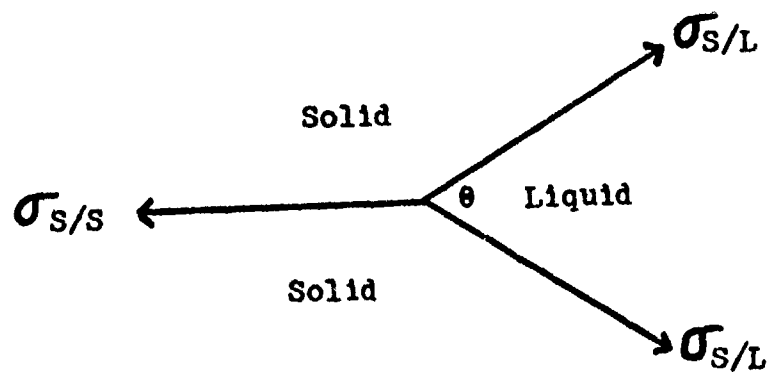


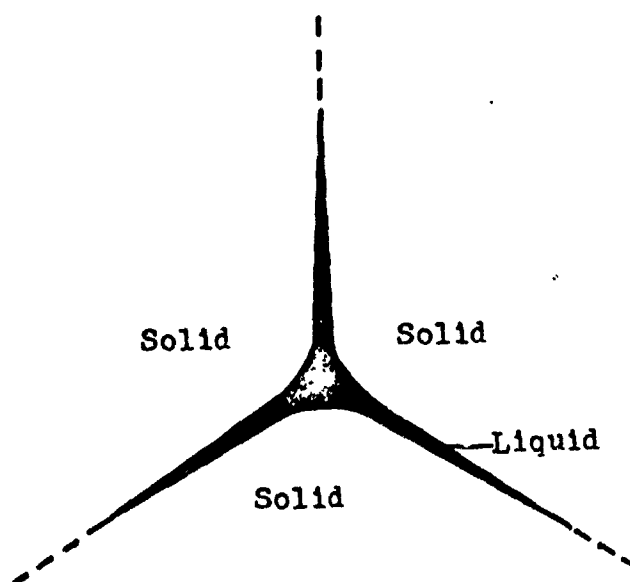
FIGURE 73. Representation of internal oxidation.  
(After Rahmel<sup>36</sup>)

/// Iron oxides

● X or Fe-X oxides



$$\sigma_{S/S} = 2\sigma_{S/L} \cos \theta/2$$



$$\theta \rightarrow 0^\circ$$

$$\sigma_{S/S} \approx 2\sigma_{S/L}$$

FIGURE 74. Criteria for liquid metal penetration at grain boundaries. (After C. S. Smith<sup>34</sup>).

## LITERATURE CITED

1. "Minigun Heat Study," General Electric Armament Department, Contract DAAF01-68-C-0194.
2. E. Raub and K. Muller, Fundamentals of Metal Deposition (Elsevier, 1967), 161.
3. "Hypervelocity Guns and the Control of Gun Erosion," NDRC Technical Report, Vol. 1, 1946.
4. Proceedings of the Interservice Technical Meeting on Gun Tube Erosion and Control, edited by I. Ahmad and J. P. Picard, Watervliet Arsenal, 1970.
5. Personal Communication: Ludwig Stiefel, Frankford Arsenal.
6. "Identification of Unknown Phase or Phases of a Cr-Mo-V Steel," C. W. Allen and H. Akita, University of Notre Dame, 1970.
7. Personal Communication: W. T. Ebihara, Weapons Laboratory, WECOM, October 1970.
8. R. W. Gurry, Trans. AIME, 188, 678, (1950).
9. G. C. Wood, Oxidation of Metals, 2, 11, (1970).
10. R. A. Rapp, Corrosion, 21, 382, (1965).
11. Kofstad, High Temperature Oxidation of Metals, Wiley, 1966.
12. J. Chipman and E. F. Brush, Trans. AIME, 242, 35, (1968).

### LITERATURE CITED (Continued)

13. N. Bredz and H. Schwartzbart, Welding Journal, p. 305-S, (1959)
14. G. Hume, L. H. Cope, and H. T. Hall, Metallurgia, April 1965, p. 169.
15. A. E. Vainerman and A. A. Gsetnik, "Fig.-Khim. Mekh. Mat.," 5, 151, (1969). Brutcher Translation 7981.
16. E. J. Eckel and S. J. Paprocki, Trans. ASM, 41, 1204, (1949).
17. Coles, Hill, Dawson, and Watson, Thermal and High Strain Fatigue, Institute of Metals, 1967, p. 270.
18. G. J. Hill, Thermal and High Strain Fatigue, Institute of Metals, 1967, p. 312.
19. E. Krempl and C. D. Walker, Fatigue at High Temperature, ASTM STP 459, p. 75, (1968).
20. L. E. Coffin, General Electric (Schenectady, N.Y.) Report 71-C-108, (1971).
21. L. E. Coffin, Trans. ASM, 56, 339, (1963).
22. M. R. Achter, G. J. Danek, and H. H. Smith, Trans. AIME, 227, 1296, (1963).
23. C. J. McMahon and L. F. Coffin, Metallurgical Trans. 1, 3443, (1970).
24. G. J. Danek, H. H. Smith, and M. R. Achter, Proc. ASTM, 61, 775, (1961).

### LITERATURE CITED (Continued)

25. P. Shahinian and M. R. Achter, Trans. AIME, 215, 37, (1959).
26. J. A. Webber, Carburizing, ASM Symposium, 1937, p. 89.
27. D. Shechtman and S. Niedzwiedz, Material Sci. and Eng. 5, 35, (1969).
28. W. W. Smeltzer, Acta Met., 8, 377, (1960).
29. W. W. Smeltzer, Trans. AIME, 218, 674, (1960).
30. F. S. Pettit and J. B. Wagner, Acta Met., 12, 35, (1964).
31. F. Pettit, R. Yinger, and J. B. Wagner, Acta Met., 8, 617, (1960).
32. C. E. Wicks and F. E. Block, "Thermodynamic Properties," Bureau of Mines Bull. 605, (1963).
33. I. S. Kozlovskii, Metal Science and Heat Treatment, 3, 157, (1967).
34. A. Hultgren and E. Hagglund, Trans. ASM, 39, 820, (1947).
35. J. L. Meijering, Acta Met., 3, 157, (1955).
36. S. S. Manson, Intl. Jnl. of Fracture Mech., 2, 327, (1966).
37. C. S. Smith, Trans. AIME, 175, 15, (1948).
38. L. H. Van Vlack, Materials Science for Engineers, Addison-Wesley, Reading Mass., (1970).

## APPENDIX A

### Results of Visual Inspection of Test Fired Barrels

<u>Barrel</u>	<u>Remarks</u>
unplated-unfired	Isolated spots of pitting (rust).
U-1	General discoloration, no residue, no bore damage.
U-10	Appearance essentially same as U-1, except completely blackened. Small amounts of residue present.
U-50	Definite copper deposits on lands and in corners of rifling. Slight pebbly roughness in corners.
U-100	Appearance essentially same as U-50.
U-200	Copper and crust distributed over entire bore surface. No visible damage to bore other than possible wearing away of rifling.
U-300	Muzzle end of barrel exhibits heavy deposits of copper which is easily flaked off. Deposits have effectively eliminated rifling at the muzzle end. Breech end of bore doesn't show much copper or crust.
U-661	Not observed.
U-900	Crust over entire bore. Copper deposits at muzzle end not nearly as heavy as in Cr Plated barrels. Moderate transverse checking on rifling in first 6". Rifling deformed -- not as pronounced as in Cr plated barrels.
U-1500	Transverse checking becoming heavier. Minimal indications of Cu at breech end. Rifling is well worn -- essentially has been eliminated in first 6" of barrel.
U-2100	Checking has advanced to more of a network. Checking continues on lands further down the barrel. Rifling is gone at breech end. Some of the network cracks show copper. A few pits developed near origin (first 1").

# APPENDIX A (continued)

<u>Barrel</u>	<u>Remarks</u>
C-1	Dull gray color with brown streaks (Cu) especially on lands and over entire bore surface on muzzle half of barrel.
C-10	About same as C-1 but more obvious.
C-50	Crust built up on muzzle 1/3. Checking network in this crust -- cannot determine if also in Cr plating. Upper 2/3 continues to be coppered. Copper also in crust area. Crust easily flakes off, copper is adherent.
C-100	Heavy, non-adherent crust at breech end. Cracking apparently developing in plating beneath crust. Rifling collecting copper. Copper in cracks appears to be pushed up giving a positive network. This occurs 5-8" from origin of rifling and is different from checking nearer breech end which doesn't exhibit copper in cracks.
C-200	Checking decorated by copper filling the cracks is visible over entire bore but is most prevalent in mid-section. First 3" seems to contain least amount of copper. Checking and copper pickup begins in corners of rifling, heavy deposits being found toward the muzzle end. Possible indication of melting of the copper in the appearance of stringers along rifling.
C-300	Definite damage at the origin of rifling where material has been removed. Also in this area can see displacement of Cr grains indicating these areas may become detached. Checking with cracks filled with copper, checking being most obvious in breech 1/3. Muzzle 1/2 has continuous heavy deposits of copper.
C-661	Not observed.
C-900	Serious damage at origin of rifling. Entire bore shows copper filled crack network. Lands remain sharp. Rounded globules of copper laying on bore (~8" from origin of rifling) taken as evidence of melting and solidification after last round.

# APPENDIX A (continued)

<u>Barrel</u>	<u>Remarks</u>
C-1500	Removal of chromium plating gives pitted appearance near breech end. Some plating grains are raised, others are depressed or caved in. Some holes do not exhibit copper, but copper does decorate cracks over entire barrel.
C-2100	Generally similar appearance as C-1500. Globular copper observed laying on surface in first inches.
C-3000	Crust and copper distribution as previous barrels. First inch of bore severely attacked Pits for first 3". Rifling is in good shape except at origin where enough of the plating has been removed to expose pebbly surface of underlying steel. Copper filling rough areas on lands but few of the pits are filled. Heavy copper deposits at muzzle end eliminate rifling.

# APPENDIX B

## X-ray Diffraction Data

C-300 first 12"		C-300 last 6"		U-300 first 12"		U-300 last 6"		C-3000 first 3"		C-3000 last 6"		U-3000 first 3"		U-3000 last 6"	
d	I	d	I	d	I	d	I	d	I	d	I	d	I	d	I
3.8	VW			3.8	VW							3.3	VW		
3.35	VW			3.1	VW	3.1	VW								
		3.0	MS	3.0	MS	3.0	MW			3.01	M			3.01	MS
3.0	M	2.83	VW	2.83	M	2.81	MW			2.81	W	2.84	W	2.85	M
2.83	VW			2.51	VW							2.51	W		
2.46	W	2.45	W	2.45	MW	2.45	M			2.45	M	2.45	VW	2.46	MS
2.32	W	2.32	W												
2.25	W	2.26	W												
2.08	VS	2.08	VS	2.27	W	2.07	S	2.08	M	2.08	VS	2.08	VW	2.08	VS
				2.09	VS			2.02	S			2.02	S		
1.91	MW	1.91	W	1.90	NW	1.90	MW							1.91	VW
1.86	MW	1.86	W	1.86	W	1.86	VW			1.9	W				
1.81	VS	1.81	S	1.81	S	1.80	MS	1.80	VW	1.80	MS			1.80	S
				1.74	W	1.73	W					1.74	VW		
1.62	VW	1.62	VW	1.62	VW									1.62	
1.59	VW	1.58	VW	1.59	VW							1.60	VW		
1.52	VW	1.52	VW	1.52	VW	1.52	VW					1.5		1.52	
1.46	VW			1.48	W	1.48	VW					1.48	W	1.48	VW
												1.43	M		
1.28	S	1.26	MS	1.28	MS	1.28	M			1.28	M			1.28	M
		1.09	MS	1.10	W	1.09	W			1.09	M			1.09	M
1.04	M	1.04	M			1.04	W	1.04	W	1.04	M			1.04	W
										1.01	W	1.01	M		
.91	MS									.91					
.83	MS	.83	M							.83	M				
.81	MS	.81	M							.81	M				

# APPENDIX C

## Normalized Intensities

Figure + 1

	1	4	6	9	12	14	16	22	26	30	31(l)	31(r)	37(l)	37(r)	38(l)	38(r)	10
Al	1	7	131	7	15	2	4	3	2	12	2	1	3	1	3	1	2
P			24														
Pb,S		11	53	9	15	2	6	6	4	8	5	2	3	2	2		5
Ca		9	195	17	17	3	6	8	5	28	5		73		4		5
Cr	4	60	92	6	6	3	9	5	4	5	4	4	3	4	4	3	4
Cr	3	28	20	6				4	3	5		3		3	3		4
Fe	100	100	100	100	100	100	100	100	100	100	100	100	100	100	100	100	100
Fe	15	18	26	17	19	15	21	15	15	16	15	21	31	15	15	15	14
Cu			50	4	8	1	5	17	2	8	3	1	590		3		
Zn			20										95		1		
Cu								12		3		1	97	1			
Pb		5	11	3	5	1	4	1	2	4	3	1		1			1
Pb				2										1			1

APPENDIX C (continued)

Actual Intensities

Figure	1	4	6	9	10	12	14	16	22	26	30	31(l)	31(r)	37(l)	37(r)	38(l)	38(r)
Al	220	170	3052	1023	585	257	108	120	687	315	1251	74	184	417	200	832	306
P	580																
Pb,S		283	1245		1335	243	114	153	1245	574	883	176	271	445	238	584	
Ca		227	4552	2368	1127	278	165	157	1685	768	3047	153		1112		1013	
Cr	916	1478	21328	916	1153	111	207	249	950	548	508	112	582	388	555	966	755
Cr	702	689	4597	818	1066				796	460	497		489	479	469	802	
Fe	22361	2474	2327	15217	25943	1678	5978	2781	20188	14466	10750	3364	14364	1530	13642	25361	23513
Fe	3330	453	614	2404	3658	320	891	604	3125	2129	1686	517	2118	479	2056	5883	3454
Cu			1159	605		126	60	140	3366	250	866	92	150	9022	201	840	
Zn			475											1452		270	
Cu									1488		294		127	1487		122	
Pb		121	266	374	571	85	71	99	292	288	440	100	156			127	
Pb				274	242											107	

# APPENDIX D EQUILIBRIUM COMBUSTION GAS COMPOSITIONS<sup>5</sup>

WC 846 AL 44065

	50,000.	25,000.	10,000.	5,000.	1,000.	14.7
T <sub>c</sub>	21119C	1810	1472	1265	943	587
P <sub>c</sub>	0.04230	0.04230	0.04220	0.04200	0.04060	0.03590
S	2.0749	2.0749	2.0749	2.0749	2.0749	2.0749

	0.9823	0.9823	0.9823	0.9823	0.9823	0.9823
H	0.9823	0.9823	0.9823	0.9823	0.9823	0.9823
C	0.3795	0.4487	0.3399	0.5496	0.2944	0.4805
O	0.9832	0.2269	0.1689	0.2769	0.6904	0.6094
N	0.5285	0.1977	0.9675	0.5668	0.3230	0.9232
HCN	0.3508	0.1605	0.1720	0.1799	0.1410	0.1156
H <sub>2</sub>	0.1531	0.1893	0.1764	0.1651	0.1828	0.2027
H <sub>2</sub> O	0.1968	0.4152	0.1871	0.2096	0.1397	0.1660
CH	0.1464	0.4342	0.4199	0.4045	0.8017	0.2768
CO	0.4419	0.7902	0.8101	0.1269	0.3529	0.1424
CH <sub>2</sub>	0.3841	0.1063	0.1208	0.1364	0.1577	0.3243
CO <sub>2</sub>	0.9861	0.5396	0.1886	0.8514	0.1892	0.3381
CH <sub>3</sub>	0.1244	0.7368	0.1879	0.4591	0.1036	0.1238
CH <sub>4</sub>	0.4912	0.2662	0.2537	0.7985	0.2197	0.2298
C <sub>2</sub>	0.2715	0.6915	0.2456	0.1163	0.1620	0.
C <sub>2</sub> H <sub>2</sub>	0.1675	0.1057	0.1273	0.2493	0.1428	0.3481
C <sub>2</sub> H <sub>4</sub>	0.5198	0.1569	0.4880	0.4370	0.4852	0.3196
C <sub>2</sub> N <sub>2</sub>	0.2203	0.3841	0.2182	0.1931	0.7514	0.1219
C <sub>3</sub>	0.2357	0.2277	0.1563	0.2342	0.9544	0.7109
OH	0.5297	0.7181	0.1836	0.8606	0.2664	0.3067
O <sub>2</sub>	0.7809	0.1211	0.3645	0.1920	0.9394	0.1327
NH	0.1129	0.5474	0.6153	0.1014	0.3190	0.2788
NO	0.2372	0.2324	0.6913	0.1014	0.1650	0.2917
NH <sub>2</sub>	0.9799	0.5292	0.4509	0.5364	0.1394	0.5381
NO <sub>2</sub>	0.6471	0.1080	0.1083	0.4163	0.2880	0.5316
NH <sub>3</sub>	0.1078	0.0	0.0	0.1089	0.1127	0.1275
N <sub>2</sub>	0.0	0.0	0.0	0.0	0.0	0.1341
(S)	0.0	0.0	0.0	0.0	0.0	0.0

COMPOSITION IN MOLE FRACTIONS

APPENDIX D (continued)

SAMPLE CALCULATION AT 943°C

<u>Reaction</u>	<u>K</u>	<u>Kcalc</u>	<u>Keq*</u>	<u>Comments</u>
(1) $\text{CO} + \text{H}_2\text{O} = \text{CO}_2 + \text{H}_2$	$\frac{(P_{\text{CO}_2})(P_{\text{H}_2})}{(P_{\text{CO}})(P_{\text{H}_2\text{O}})}$	.70	.69	gas components in equilibrium
(2) $\text{CO} + \text{FeO}_x = \text{CO}_2 + \text{Fe}$	$\frac{(P_{\text{CO}_2})}{(P_{\text{CO}})}$	.53	.43	excess $\text{CO}_2$ -oxidizing pressure independent
(3) $\text{H}_2 + \text{FeO}_x = \text{H}_2\text{O} + \text{Fe}$	$\frac{(P_{\text{H}_2\text{O}})}{(P_{\text{H}_2})}$	.76	.64	excess $\text{H}_2\text{O}$ -oxidizing pressure independent
(4) $\text{C} + \text{CO}_2 = 2\text{CO}$	$\frac{(P_{\text{CO}})^2}{(A_{\text{C}_Y})(P_{\text{CO}_2})}$	163	70	excess CO-carburizing increasing pressure shifts reaction to more carburizing
(5) $\text{C} + 2\text{H}_2 = \text{CH}_4$	$\frac{(P_{\text{CH}_4})}{(A_{\text{C}_Y})(P_{\text{H}_2})^2}$	.035	.016	excess $\text{CH}_4$ -carburizing increasing pressure shifts reaction to less carburizing

\* Values for Keq and  $A_{\text{C}_Y}$  (activity of carbon in austenite) were obtained from R. W. Gurry, Trans. AIME, 188, 678, 680 (1950).